EurJOC
European Journal of Organic Chemistry

Full Papers
doi.org/10.1002/ejoc.202100948

Chemistry Europe
European Chemical Societies Publishing

Special Collection

A Comprehensive Study of the Ca^{2+} Ion Binding of Fluorescently Labelled BAPTA Analogues

Attila Csomos,[a] Bence Kontra,[a] Attila Jancsó,[b] Gábor Galbács,[b] Ruth Deme,[c] Zoltán Kele,[d] Balázs József Rózsa,[e, f] Ervin Kovács,*[a, g] and Zoltán Mucsi*[a, h]

In memory of Ferenc Fülöp.

Since its development, the ionophore BAPTA (1,2-bis(2-aminophenoxy)-ethane-N,N,N′,N′-tetraacetic acid) has been used unchanged in calcium sensing applications. In this work we present a comprehensive experimental and theoretical study of novel alterations in the structure of BAPTA, with a focus on the systematic modification of the chain connecting the two aromatic rings of the molecule (denoted as "linker"). A bis-(diethylamino)xantene fluorophore was also attached to the structures in a fixed position and the structure-fluorescence response relationship of these molecules was investigated in addition. The effect of the linker's length, the number of oxygen atoms in this chain and even the removal of one of the rings was tested; these all proved to significantly alter the characteristics of the compounds. For example, it was found that the second aromatic ring of BAPTA is not essential for the turn-on of the fluorescence. We also demonstrated that successful sensing can be realized even by replacing the chain with a single oxygen atom, which suggests the availability of a new calcium binding mode of the chelator. The reliable turn-on characteristic, the steep Ca^{2+} fluorescence titration curve and the intense fluorescence emission combine to make this compound a prospective candidate as a calcium sensing molecular probe in diagnostic neurobiological applications.

Introduction

Calcium ions play an essential role in multiple physiological processes e.g in muscles, various organs, and parts of the nervous system. Examples include signal transduction, gene transcription and blood coagulation, among others.[1] Furthermore, the omnipresence of Ca^{2+} ions has contributed substantially to the success of imaging over the last 40 years. Understanding cellular processes by monitoring the presence of Ca^{2+} ions at the cellular level was made widely available by the introduction of the visually active ionophore 1,2-bis(2-aminophenoxy)-ethane-N,N,N′,N′-tetraacetic acid (BAPTA, **1a**) in the pioneering work of Tsien *et al.*[2] Since then, a wide range of BAPTA derivatives were prepared and used in biological research.[3] Lately, with the spread of genetically encoded calcium indicators, the use and the development of small molecular probes were slightly relegated into the background. Nevertheless, the latter have several advantages over the genetically encoded indicators as they offer a wider choice of Ca^{2+} affinity, display unique spectral properties and can even be used simultaneously.[3] These advantageous features allow highly customizable measurements to be executed. In addition to this, synthetic molecular probes are also suitable for subcellular Ca^{2+} imaging,[4] and recent studies also revealed possibilities for using them as MRI contrast agents[5,6] or therapeutic compounds.[7] In combination with microendoscopes,[8] fluorescent Ca^{2+} chelators also have a bright future in the fields of human diagnostics and therapy – which are applications where – the use of genetically encoded indicators is not a viable option. Despite their above highlighted importance, the development of small Ca^{2+} sensors

[a] A. Csomos, B. Kontra, Dr. E. Kovács, Dr. Z. Mucsi
Department of Chemistry, Femtonics Ltd.
1094 Budapest, Hungary
E-mail: ervin.kovacs@femtonics.eu
zmucsi@femtonics.eu
[b] Dr. A. Jancsó, Dr. G. Galbács
Department of Inorganic and Analytical Chemistry,
University of Szeged
Szeged 6720, Hungary
[c] Dr. R. Deme
Department of Organic Chemistry, Semmelweis University,
Budapest H-1092, Hungary
[d] Dr. Z. Kele
Institute of Medical Chemistry, University of Szeged
Szeged H-6720, Hungary
[e] Dr. B. J. Rózsa
Two-Photon Measurement Technology Research Group,
The Faculty of Information Technology, Pázmány Péter Catholic University
Budapest 1083, Hungary
[f] Dr. B. J. Rózsa
Laboratory of 3D Functional Imaging of Neuronal Networks and Dendritic Integration,
Institute of Experimental Medicine
Budapest, 1083, Hungary
[g] Dr. E. Kovács
Polymer Chemistry Research Group,
Research Centre for Natural Sciences
Budapest, 1117, Hungary
[h] Dr. Z. Mucsi
Faculty of Materials Science and Engineering, University of Miskolc
Miskolc 3515, Hungary

Supporting information for this article is available on the WWW under https://doi.org/10.1002/ejoc.202100948

Part of the Special Collection in memory of Ferenc Fülöp.

based on fluorescent chelators has received little attention lately.

For the purpose of fluorescent Ca^{2+} imaging, the BAPTA (**1 a**) ionophore can be coupled to a wide range of fluorophores thereby producing a large number of different dyes (a few important examples shown in Figure 1, bottom) with potential uses in several applications.[9] In this work, we present our efforts to optimize the BAPTA ionophore scaffold for fluorescent Ca^{2+} imaging and to discuss the structure-activity relationship of the modifications on the chelating and spectrophysical properties of the complexes.

The substituent effects on the aromatic rings of BAPTA (**1**, Figure 1) were widely investigated earlier by Pethig and co-workers.[10] Kimura *et al.*[11] have measured the affinity of the ionophores towards Ca^{2+}, which decreased radically with the enlargement of the binding pocket by extending the linker of the compound (*e.g.* **3 a**, BAPPTA in Figure 1). Analogous molecular probes for Ca^{2+} detection by NMR, known as AATA (**2 a** in Figure 1) were also developed. In this case one of the aromatic rings was replaced with ethylene, combining the features of BAPTA and EGTA.[12] However, in none of these studies was the coupling of the ionophores to fluorophores accomplished. This motivated us to investigate the effects of the linker on the Ca^{2+} complexation and the fluorescence property in a comprehensive study.

This work discusses three known (**1 a**, **2 a**, **3 a**) and four novel chelating scaffolds (**4 a**–**7 a**) containing the same tetraethyl rhodamine fluorophore (rosamine analogues, summarized in Figure 1 as **1 b**–**7 b**). The tetraethyl rosamine fluorophore was selected because it exhibits better two-photon absorption than the tetramethyl variant (TAMRA) which is beneficial for further biological applications.[13,14] This set of modified fluorescent ionophores were subjected to a spectroscopic investigation combined with fluorescence-monitored Ca^{2+}-titrations in order to study the details of their interaction with Ca^{2+} ions. In particular, the optimal length of the linker and the role of the oxygen atom with regards to Ca^{2+} affinity were studied along with the photophysical changes of the fluorescent dyes (**4 b**–**7 b**). For comparative purpose, derivatives of the original and longer ionophore analogues (BAPTA and BAPPTA, **1 b** and **3 b**) were also prepared and studied in the same way. The photophysical characteristics of the fluorescent derivatives of AATA (**2 b**) were not reported in the literature earlier, therefore we investigated our novel construction as well.[15] This fluorophore unit lacks the possibility of regioisomer formation, and it is easily attachable to the scaffolds.[16]

In summary, our aim was the synthesis of seven novel compounds (**1 b**–**7 b**, Figure 1) to investigate the relationship between their structure and fluorescence properties induced by Ca^{2+} binding.

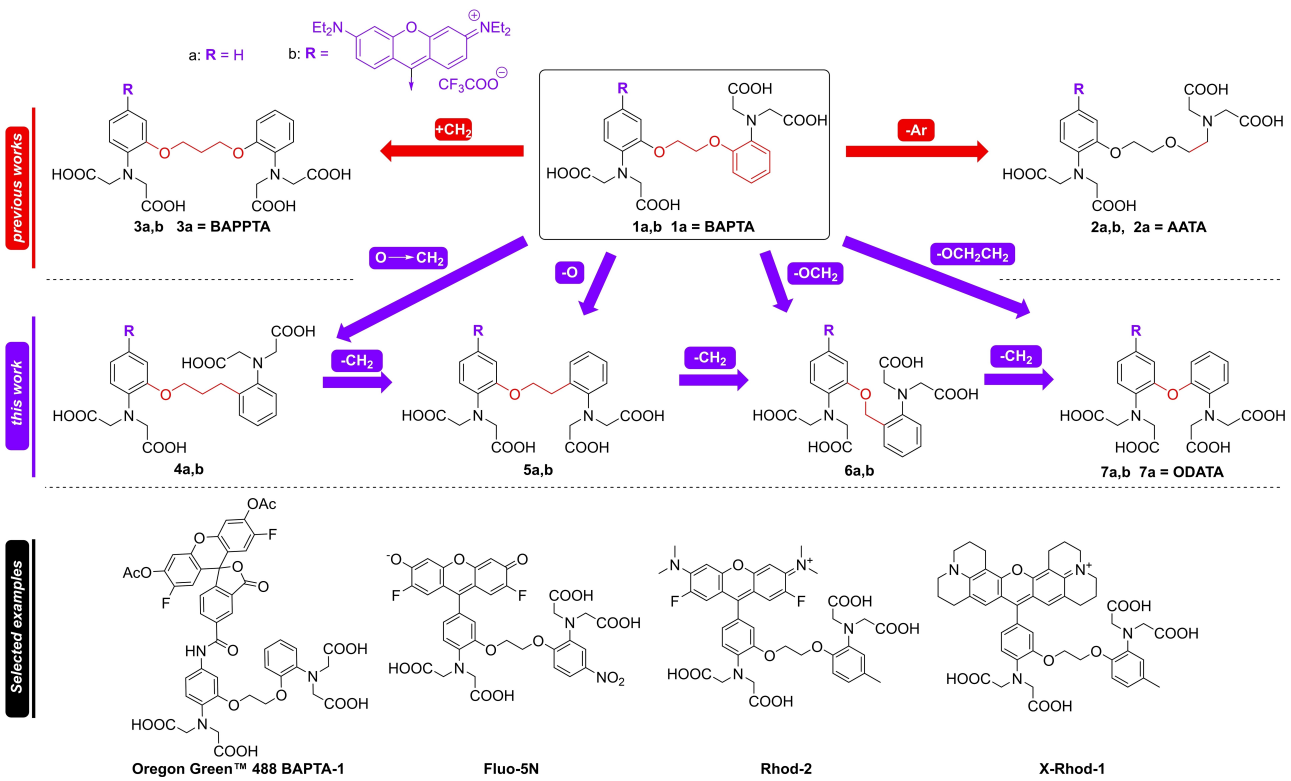

Figure 1. Top: The concept of the present study. Systematic modification in of the BAPTA (**1**) structure using shorter linkers (**4**, **5**, **6**, **7** = ODATA), than the previously reported modifications (**2**) as well as a derivative with a single phenyl group (**3**, AATA). Bottom: a few selected examples of the available fluorescent dyes based on BAPTA.[9]

Results and discussion

Chemical Synthesis

Tetraethyl ester derivatives of BAPTA (**1a**) and BAPPTA (**3a**) were prepared as previously reported (see Scheme S1 in the supplementary information).[2,11] Tetraethyl ester of AATA was synthesized by a more productive way compared to the previous attempts (Scheme 1).[15] The original azide formation and reduction steps were replaced by N-alkylation of diethyl iminodiacetate using compound **8**, followed by a reduction and further alkylation, which produced the desired ester of AATA (**11**).

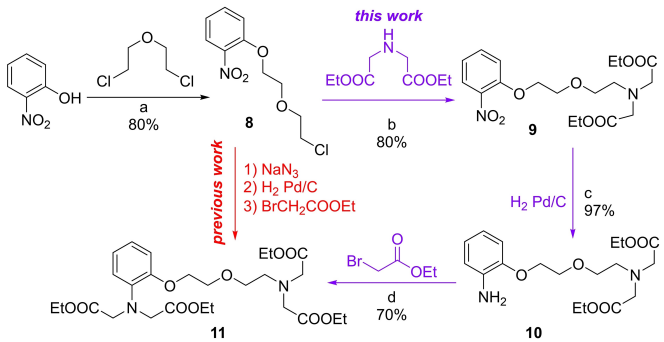

Scheme 1. Preparation of the tetraethyl ester of AATA (**11**). a: 1.5 equiv. K_2CO_3, DMF, 110 °C, 2 h, b: 1.5 equiv. DIPEA, DMF, 110 °C, 144 h, c: H_2 (10 bar), 10% Pd/C, EtOH, RT, 2 h. d: 6 equiv. Na_2HPO_4, 0.2 equiv. KI, MeCN, reflux, 10 h.

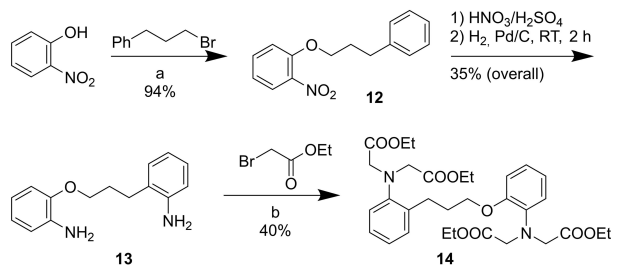

Scheme 2. Synthetic route to **14**. a: 2 equiv. K_2CO_3, DMF, 110 °C, 2 h, b: 6 equiv. Na_2HPO_4, 0.2 equiv. KI, DMF, 90 °C, 12 h.

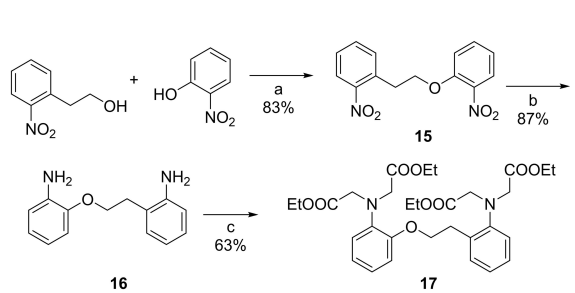

Scheme 3. Synthetic route to the tetraethyl ester **17**. a: 1.1 equiv. PPh_3, 1 equiv. DIAD, abs. THF, 0 °C→RT, 1 h, recrystallisation, b: H_2, 10% Pd/C, RT, d: 6 equiv. $BrCH_2COOEt$, 6 equiv. Na_2HPO_4, 0.2 equiv. KI, DMF, 12 h.

Preparation of the ester of **4a** was carried out from 2-nitrophenol by an alkylation followed by nitration, and reduction (Scheme 2).

For the synthesis of the ionophore **5a**, the Mitsunobu reaction, a reduction and an alkylation step proved to be an effective route providing intermediate **17** with a good yield (Scheme 3).

For the preparation of **20**, after the O-alkylation (**18**), PtO_2 was applied to an effective catalyst[17] to avoid the unwanted benzylic cleavage instead of reduction. However, amine **19** is extremely sensitive to oxidation and was found to decompose at elevated temperatures during the alkylation. To avoid this, DMF solvent was used at a lower temperature (70 °C). The desired product (**20**) formed with a moderate yield after 15 hours (Scheme 4).

The tetraethyl ester of oxydianylinyl N,N,N′,N′-tetraacetic acid (ODATA, **7a**) was prepared by employing a method reported in the literature (Scheme S2).[2,18] In the next synthetic step, the formyl group was introduced into one of the benzene rings of **11**, **14**, **17**, **20**–**23**, to allow the attachment of the rhodamine moiety to the molecule,[19] according to a well-described procedure (Scheme 5).[16]

Spectroscopic Characterization

Fluorescence spectra of each fluorescent Ca^{2+} chelating candidates (**1b**–**7b**) were recorded in samples containing the compounds in a $c < 1$ μM concentration and at pH = 7.4 (MOPS buffer). Spectra were acquired in the absence as well as in the presence of Ca^{2+} ions the concentration of which was set to a high, but biologically relevant level (37 μM) with a Ca^{2+}-buffer, EGTA. Figure 2 shows that the shape and position of the fluorescence emission bands of these compounds are very similar, with significant differences present only in their intensities. All spectra recorded in the absence of metal ions reflect very weak emissions.

The intensity enhancements observed in the presence of Ca^{2+} ions suggests that all compounds bind Ca^{2+} ions to some extent and that the binding is followed by a change in their photophysical properties. This turn on change can be explained by Ca^{2+} induced diminishing of the photoinduced electron

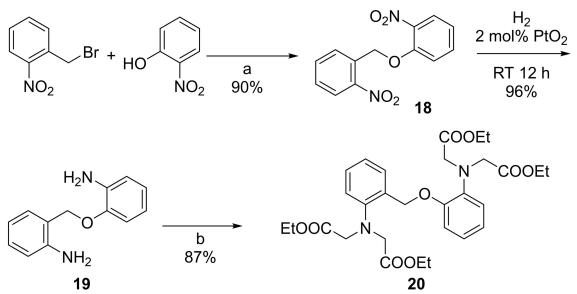

Scheme 4. Synthetic route to the tetraethyl ester of **6b**. a: 1.2 equiv. NaH, DMF, RT→90 °C, 6 h, b: 6 equiv. $BrCH_2COOEt$, 6 equiv. Na_2HPO_4, 0.2 equiv. KI, DMF, 70 °C, 15 h.

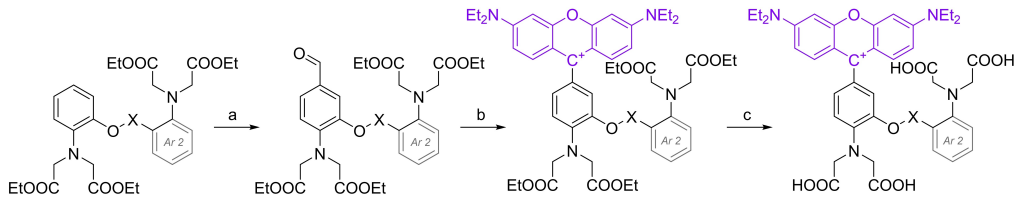

X =	Ar 2	Comp.	Comp.	Yield	Comp.	Yield	Comp.	Yield
	✓	21	24	42.5	31	20	1b	62
	X	11	25	35	32	18	2b	90
	✓	22	26	45	33	22	3b	85
	✓	14	27	28	34	15	4b	54
	✓	17	28	82	35	6	5b	41
	✓	20	29	22	36	15	6b	94
	✓	23	30	50	37	24	7b	93

Scheme 5. General synthetic route to achieve the desired fluorescent Ca^{2+} molecular probes (**1b**–**7b**). a: 1.2 equiv. $POCl_3$ in DMF, 85 °C, 3 h. b: 1) 2 equiv. 2-(diethylamino)phenol in propionic acid, 110 °C, 4 h. 2) 0.95 equiv. chloranil in EtOH, RT, overnight, c: 8 equiv. aqueous NaOH 20% in 5 ml EtOH, RT, 30 min.

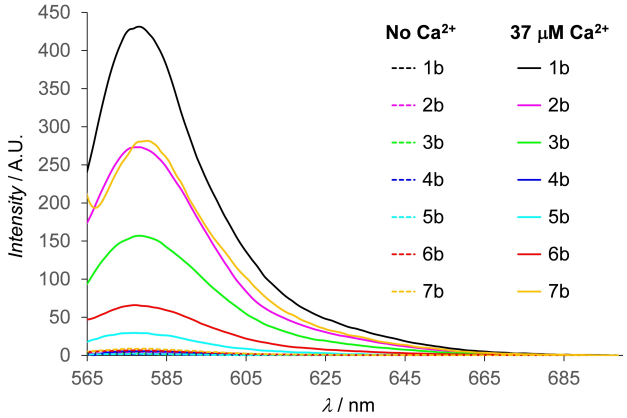

Figure 2. Fluorescence spectra of the prepared compounds in solutions containing no Ca^{2+} ions (dashed lines) and 37 μM free Ca^{2+} ions (continuous lines). Spectra were recorded at pH = 7.4 (MOPS buffer) and normalized to 1.0 μM concentrations of the compounds.

transfer (PET) mechanism operating otherwise in the metal ion free form of the molecules.[20] The observed fluorescence enhancement factors (FEF) are between ca. 3.5 and 120 (see Table 1). Although this confirms that all compounds show some response to Ca^{2+}, the increase in the fluorescence activity covers a broad range. The observed values reflect that none of these molecular probes are capable to overperform the BAPTA derivative (**1b**). Out of the longer ionophore derivatives, AATA (**2b**), BAPPTA (**3b**) and **4b**, **2b** shows a notably larger fluorescence enhancement. The probes, based on a shorter ionophore design (**5b**–**7b**), display a rather mixed fluorescence response for Ca^{2+} ions. The observed fluorescence enhancements measured for **4b**, **5b** and **6b** are rather low (**4b**) or modest (**5b**, **6b**). The compound containing only one oxygen as a linker (**7b**) exhibits the second largest FEF, on par with **2b**, only superseded by the original BAPTA-derivative (**1b**).

To gain a more detailed insight into the Ca^{2+} ion promoted fluorescence response of the investigated compounds and about their affinity towards Ca^{2+} ions, Ca^{2+}-titrations were performed with all seven candidate molecules by recording their fluorescence emission spectra in a series of solutions containing the studied compound in a constant concentration and Ca^{2+} ions in gradually increasing concentrations. The Ca^{2+} concentrations were adjusted following a widely used protocol using EGTA as a Ca^{2+}-buffer, while the pH was kept at physiologically relevant value of 7.2 (MOPS) and the ionic strengths at 0.1 M (KCl).[21,22] The fluorescence intensity values

Table 1. Measured spectroscopic properties of the prepared compounds without Ca^{2+} ion (and in the presence of Ca^{2+} ion).[a]

	λ_{abs} [nm] (Ca^{2+})	ε [$M^{-1}\times cm^{-1}$] (Ca^{2+})	F_{max}/AU	FEF[b]	QY (Ca^{2+})[c]	λ_{em} [nm] (Ca^{2+})[d]	p[Ca^{2+}][e]
1b	555 (559)	8.49×10^4 (9.37×10^4)	432	122	0.001 (0.113)	575 (578)	6.1
2b	553 (559)	5.67×10^4 (5.91×10^4)	273	93	0.001 (0.117)	575 (578)	5.8
3b	554 (557)	7.22×10^4 (7.81×10^4)	157	65	0.001 (0.052)	577 (578)	5.4
4b	554 (554)	8.06×10^4 (8.46×10^4)	5.4	3.5	< 0.001 (0.001)	573 (577)	≪5[f]
5b	554 (554)	7.51×10^4 (7.88×10^4)	29.3	14	< 0.001 (0.009)	577 (577)	≪5[f]
6b	553 (554)	9.63×10^4 (1.04×10^5)	65.9	10	0.002 (0.015)	578 (577)	≪5[f]
7b	555 (561)	8.57×10^4 (8.85×10^4)	281	32	0.002 (0.077)	581 (580)	5.7

[a] Data published here (pH = 7.20 (MOPS); I = 0.1 M KCl; T = 25 ± 0.1 °C. Fluorescence intensities (F_{max}) are normalized to c = 1.0 μM concentrations of the studied compounds. [b] Fluorescent enhancement factor: $(F_{max}-F_0)/F_0$. F_0 and F_{max} are the fluorescent intensity observed without (F_0) and in the presence (F_{max}) of Ca ion. [c] Fluorescence quantum yields (QY) were estimated based on the method described by Lakowicz[20] [d] Wavelength of the intensity maximum of the emission bands in the absence and presence of Ca^{2+} ions. [e] p[Ca^{2+}] values at the half of the overall fluorescence intensity change observed in the Ca^{2+}-titration procedure. [f] These values are below the experimental measurement limit and can be significantly smaller due to the assumed incomplete fluorescence change by the end of the titration process terminating at [Ca^{2+}] = 37 μM.

observed at the maxima of the emission bands plotted against the concentration of Ca^{2+} ion at logarithmic scale produce classical fluorescence titration curves, as depicted in Figure 3. The inflection points of such curves may provide a good estimation of the apparent dissociation constants of the complexes if the shape of the curve represents a simple one-step association process completed by the end of the titration protocol, such as that of the BAPTA-derivative (**1b**).

The titration curves of **1b**, **2b** and **7b** clearly have a sigmoidal shape with saturating fluorescence intensities at the far end of the concentration scale, suggesting that the Ca^{2+}-binding event is completed within the concentration range of the titrations and that the compounds are characterized by Ca^{2+}-binding affinities falling in the $pK'_d = 5.6–6.2$ range (Figure 3). These values, including the $p[Ca^{2+}] = 5.7$ for the Ca^{2+}-binding step of **7b** (Table 1) are rather high and indicate remarkable Ca^{2+}-sensitivities of these sensor candidates. The steeper and more distinguished increase in the curve of **7b** offers better usability in neurobiological applications, where the binary (active/inactive) signalling is preferred in contrast to the exact determination of the Ca^{2+} concentration.

Interestingly, the observed fluorescence response steps are rather steep for many of the studied compounds suggesting differences in their Ca^{2+}-binding mechanisms as compared to the BAPTA-based molecular probe. At the same time, titration curves of other compounds might indicate that the complexation process is not complete. Both are interesting phenomena that may initiate further investigations but are out of the scope of the present study. For the characterization of the Ca^{2+}-binding abilities of the investigated compounds we used the $p[Ca^{2+}]$ values at the inflection points (where relevant) or at the half of the overall fluorescence change observed by the end of the titration protocol (see the last column in Table 1).

Compound **3b** displays an intense Ca^{2+}-promoted response around $p[Ca^{2+}] \sim 5.3–5.4$, however, the continuous increase of fluorescence even at the far end of the applied concentration range suggests a more complex metal ion binding mechanism. The observed poor performance of **4b**, **5b** and **6b** suggests

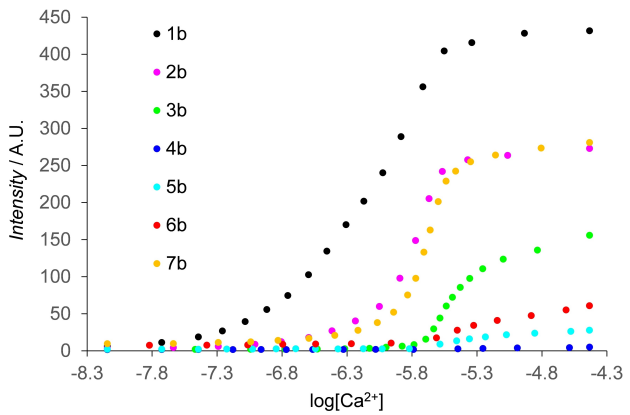

Figure 3. Titration curves representing the normalized fluorescence intensities at the maxima of the emission bands of the studied compounds as a function of the free Ca^{2+} concentrations, set by the Ca^{2+}-buffer EGTA according to the protocol described previously.[21,22]

that these compounds either possess weak affinity towards Ca^{2+}, preventing to reach fluorescence saturation in the studied concentration range, or the PET quenching of the fluorophore moiety, induced by the attached ionophores, is not fully obstructed upon Ca^{2+}-binding.

The main difference between **7b** (ODATA) and the other three novel analogues (**4b**–**6b**) is that both aromatic rings in **7b** are connected to an oxygen atom, just like in **1b**–**3b**. In contrast, the second aromatic ring in **4b**–**6b** is connected to an aliphatic chain. It would seem rational that only the fluorophore-linked aromatic ring is responsible for the quenching of fluorescence in the absence of Ca^{2+} ions, and the fluorescence turns on when Ca^{2+} ions are coordinated. However, our data imply that the more distant ring also contributes to the quenching, which is not abolished if the potential Ca^{2+}-binder, ring-connected oxygen atom is missing. The question, whether the weak fluorescence enhancement is the result of weak Ca^{2+}-binding or the inefficient induction of fluorescence via Ca^{2+}-coordination (via breaking down the internal PET) or both, cannot be unambiguously answered based on these results. It is possible that the fluorescence of these compounds may further increase at even higher Ca^{2+} concentrations, *e.g.* via a more complex metal binding scheme. Nevertheless, too low pK_D values are not relevant for the intended use of these molecular probes, i.e. in general biological applications.

Finally, we can draw the conclusion that the molecular probe based on the original BAPTA (**1b**) has the highest and optimal affinity towards Ca^{2+} and the largest fluorescence enhancement factor via Ca^{2+}-binding, however, it is closely followed by the new molecular probes **2b** and **7b**.

Theoretical Studies

A study of the Ca^{2+} ion affinity of the prepared chelators (**1a**–**7a**) at M06-2X/6-31G(d,p) level of theory is presented, aiming to shed light on the causes of the differences in the Ca^{2+} binding with regard to alterations in the structures. Previous computational works have not addressed BAPTA-based chelators. Our study revealed that the optimal conformations of complex **1a**-Ca^{2+} is different in solvents of different polarity. DFT structure optimalization *in vacuo* predicted an asymmetrical, hexacoordinated structure for this complex, with a benefit in enthalpy as large as 14.4 $kJ \cdot mol^{-1}$ (process shown in Figure 4) compared to the symmetrical (octacoordinated) arrangement. This hexacoordinated structure motivated the synthesis of new derivatives containing one linker O atom.

In other implicit solvent models presented in Figure 4, however, the preferred arrangement is the symmetrical and octacoordinated structure, which finally reaches a significant enthalpy benefit of 26.3 $kJ \cdot mol^{-1}$ in water as a solvent (Figure 4). Using the symmetrical conformation as a reference, our hypothesis for the process shown in Figure 4 was investigated for water, MeCN, THF, benzene and heptane. An exponential relation between the relative stability of the asymmetrical complex and the dipole moment of the solvent was calculated (favouring the symmetric structure in polar solvents). This

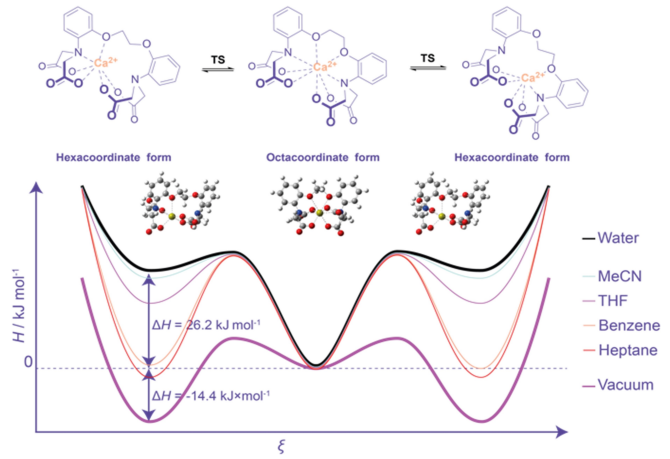

Figure 4. Solvent-dependent energy diagram of the binding process. The absolute enthalpy of the octacoordinated complex was taken as a reference in all solvents and enthalpies of the hexacoordinate forms were compared to this, by the implicit solvent model at M062X/6-31G(d,p) level of theory.

finding is in accordance with the experimental results showing a weaker binding ability of derivatives **4b**–**7b**.

In the next step, structural optimizations were carried out on the disodium (model for the non-complexed form) as well as monocalcium complexes of **1a**–**7a** and EGTA separately, to avoid the change of the overall charges. Despite BAPTA (**1a**) shares structural motifs with EGTA, their thermodynamic stability constants corresponding to Ca^{2+} binding have a difference of ca. four orders of magnitude (i.e. $pK_{D,\ BAPTA} = 6.97$ ($T = 22\,°C$) versus $pK_{D,\ EGTA} = 10.97$ ($T = 20\,°C$).[23] In order to approach the theoretical bases of this large deviation in pK_D for Ca^{2+}-binding caused by the significant difference in the basicity of the two amino functions in the two ligands,[23] we compared the enthalpy difference ($\Delta\Delta H$) of the Ca^{2+} binding of BAPTA and EGTA. According to quantum chemical calculations (Figure 5, top), the enthalpy difference of complexation is 30.4 kJ mol^{-1} in favour of EGTA. This matches the expected value based on the reported difference of $\Delta pK_D \sim 4$, which corresponds well to *ca.* 25 kJ·mol^{-1} Gibbs free energy and approximately 25 kJ·mol^{-1} enthalpy difference at room temperature.

To highlight the structure-activity relationship for the Ca^{2+}-binding of BAPTA and EGTA, we split the overall enthalpy changes into different sub-effects caused by the various functionalities (A, B and C). First, the conformational change of the ethylene linkers was studied (A), which turns from all-trans (**38a** and **38b**) to gauche (**39a** and **39b**, Figure 5A) in the course of the complexation process, resulting only a negligible ($\Delta\Delta H_A = -8.4 + 7.8$ kJ·mol^{-1} $= -0.6$ kJ·mol^{-1}) difference in favour of EGTA. Second, a larger difference was assigned to the hybrid state change of the coordinating nitrogen atom (B, Figure 5B). In the EGTA model (**39a**), the nitrogen atom retains its pure sp^3 state (pyramidity ~333–335°) during the complexation. In contrast, the nitrogen atom in the BAPTA model (**39b**) is in a mixed sp^2–sp^3 state due to the strong conjugation with the benzene ring (pyramidity = 344°), which transforms into an sp^3 state during the metal ion binding, while the above-mentioned conjugation vanishes. The computation resulted in a $\Delta\Delta H_B = -6.3$ kJ·mol^{-1} energy benefit for the EGTA model,

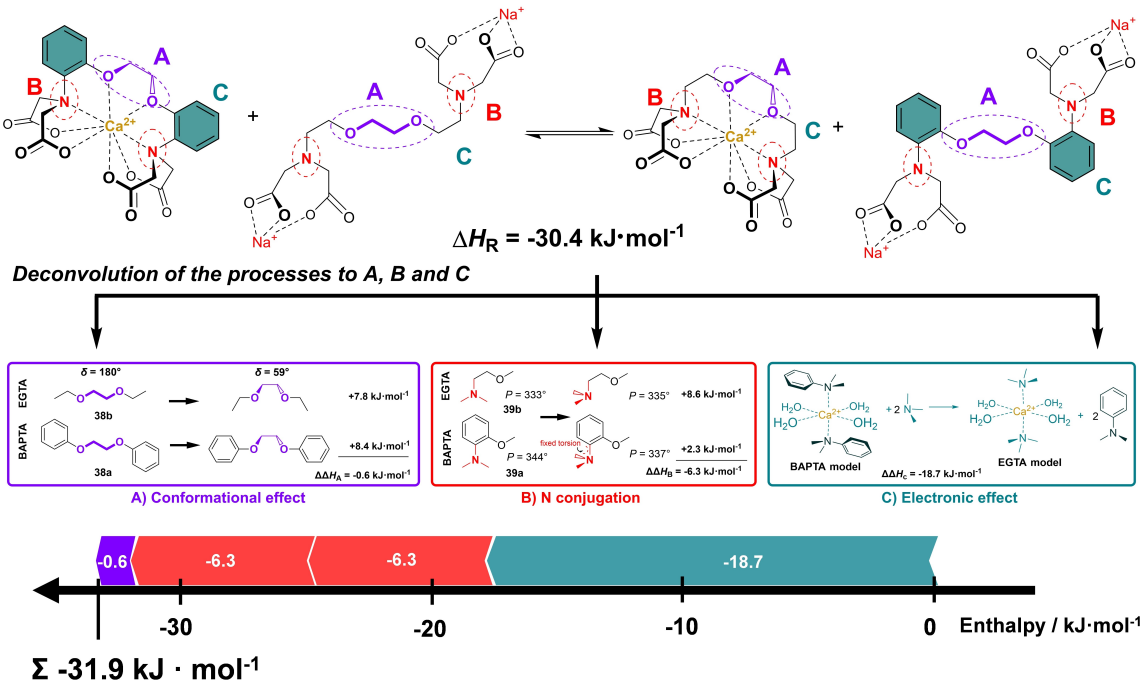

Figure 5. Complexation process of calcium ion by EGTA in the presence of BAPTA. This process is modelled by the deconvolution of three main processes as **A**: conformational changes, **B**: nitrogen conjugation differences, **C**: electronic effects. The corresponding enthalpy values were calculated at M062X/6-31G(d,p) level of theory.

confirming that the effect of conjugation (**B**) is one of the major causes of EGTA being a stronger ionophore. Third, the effect of difference in the electronic environment of the N atom (C, Figure 5C, inset) was investigated as another potential reason behind the strength of EGTA. In the proposed reaction scheme the Ca^{2+}-tetraqua-*bis*-dimethylaniline complex exchanges ligands to form the Ca^{2+}-tetraaqua-*bis*-trimethylamine complex. The enthalpy difference of this process is highly endothermic ($\triangle\triangle H_C = -18.7\ kJ \cdot mol^{-1}$). By taking everything into account, the total enthalpy effects sum up to $\Sigma\triangle\triangle H = -31.9\ kJ \cdot mol^{-1}$, which corresponds excellently to the value computed for the two Ca^{2+} complexes. In conclusion, we proved *in* silico, that the difference between the complexation of BAPTA and EGTA can be explained by the characteristics of the aliphatic and aromatic N atoms, i.e. their different basicity. It was shown that an aliphatic N atom has a larger attraction to Ca^{2+}, than an aromatic one. At pH = 7.2, however, the competing protonation equilibrium decreases this difference and the conditional stabilities of the Ca^{2+}-binding of EGTA and BAPTA are nearly identical at this pH.[23]

We estimated the enthalpy difference between the protonation of EGTA and BAPTA by model calculation (see SI, $-35.0\ kJ \cdot mol^{-1}$) which indicates that EGTA can be protonated more easily than BAPTA (column B in Table 2). The analogous thermodynamic values (*H* and *G*), calculated for the Ca^{2+}-complexation of **2a**–**7a** relative to BAPTA, are listed in Table 2. These were calculated according to the same equation. Most of the calculated enthalpies are in a good agreement with the experimental values, except for those of **3a** and **7a**.

Based on the similar equilibrium enthalpies in Table 2 for the Ca^{2+} complexation of EGTA and BAPTA it can be assumed that they possess the same coordination mode (8-coordination) and one aliphatic N atom of **2a** can produce the same effect as two in **1a**. However, the competing protonation process on the aliphatic N in EGTA decreases the overall pK_D similar to that of BAPTA. Interestingly, the sign of the calculated entropy change is the opposite in these two cases (EGTA and **2a**). The computation for the compound bearing a longer linker (**3a**) significantly underestimates the complexation enthalpy, compared to the experimental results. The predicted weak binding of **3a** to Ca^{2+} could be due to the decrease of the coordination number to 7. In our *in silico* model one of the etheric O atoms does not coordinate to Ca^{2+}. Similarly, compounds **4a**, **5a** and **6a** also lack the second O atom, and thus the largest possible coordination number for Ca^{2+} ion is 7, hence the relative enthalpies of the corresponding complexation processes are endothermic. Interestingly, the best fitting among **4a**, **5a** and **6a** was found for **4a** that has the same linker length as BAPTA (Figure 6). For **7a**, the calculated unbeneficial binding enthalpy and the corresponding ΔpK_D values are in sharp contrast with the experimental observation, as this compound experimentally displayed efficient Ca^{2+} binding ability. To resolve this contradiction, one can look for alternative binding possibilities. Supposing a possible dimer complex formation proposed in Figure 6 resulted in a more beneficial enthalpy value (Table 2).

Conclusion

In this study, a systematic structural modification of the BAPTA ionophore was performed and seven new fluorescent BAPTA-analogues were successfully synthesized and subjected to spectrophysical characterization. The excitation and emission wavelength values in addition to the absorption and emission intensities were studied in the presence and absence of Ca^{2+} ions. The affinities of the compounds towards the desired analyte ion were characterized based on fluorescence-monitored Ca^{2+} titration data. Our structure-activity relationship results suggest that even a ring at greater distance is able to quench the fluorescence in the presence of Ca^{2+} ions if there are no oxygen atoms directly connected to this ring. A comprehensive computational study was executed to reveal further information regarding the role of the structure in the complexation process. The optimal structure of the complexes depends on the polarity of the applied solvent model continuum. In apolar solvents or vacuum, an asymmetric hexacoordinated form is preferred. On the other hand, in polar models, the symmetric octacoordinated arrangement becomes preferable. The structural analysis confirmed that the hybrid state and the electronic environment of the coordinating N

Table 2. Enthalpy (ΔH in kJ mol^{-1}), Gibbs free energy (ΔG in kJ mol^{-1}) and entropy (ΔS in kJ mol^{-1} K^{-1}) values for the Ca^{2+} complexation [A], protonation [B] and their sum [A + B = C], of the aliphatic amine EGTA and **2a**–**7a** relative to BAPTA (**1a**). The calculated pK_D data are compared to experimental values.

	Coord. number	Complexation [A]			Protonation at pH = 7.4 [B]		Sum [A + B = C]		ΔpK_D	pK_D	$p[Ca^{2+}] \sim pK_D$
		ΔH_R	ΔG_R	ΔS_R	ΔH_P	ΔG_P	ΔH_R	ΔG_R	theoretical	theoretical	experimental
1a	8	0.0	0.0	0.0	0.0	0.0	0.0	0.0	0.0	*6.1*[a]	6.1
EGTA	8	−30.4	−24.4	−19.9	35.0[b]	36.7 [b]	4.6	−0.2	−0.1	6.2	6.7 [c]
2a	8	−37.9	−42.1	13.8	35.0[b]	36.7[b]	−2.9	−5.4	−0.9	7.0	5.8
3a	8	38.6	27.2	38.4	0.0[d]	0.0[d]	38.6	27.2	4.8	1.3	5.4
4a	7	25.4	15.1	34.5	0.0[d]	0.0[d]	25.4	15.1	2.7	3.5	$\ll 5$[e]
5a	7	56.3	41.7	48.7	0.0[d]	0.0[d]	56.3	41.7	7.3	−1.2	$\ll 5$[e]
6a	7	43.1	26.4	55.9	0.0[d]	0.0[d]	43.1	26.4	4.6	1.5	$\ll 5$[e]
7a	7	60.3	38.8	71.9	0.0[d]	0.0[d]	60.3	38.8	6.8	−0.7	5.7
	dimer[f]	0.1	19.9	−66.5	0.0[d]	0.0[d]	0.1	4.9*	0.9	5.2	

[a] Experimental value used as reference value; [b] According to model calculation, see SI; [c] Literature data; [d] Only anilinyl moiety, no difference in protonation to BAPTA (**1a**); [e] Much below the current experimental measurement limit; [f] For **7a**, two types of complex formation were considered, a mono complex and a dimer species, see Figure 6.

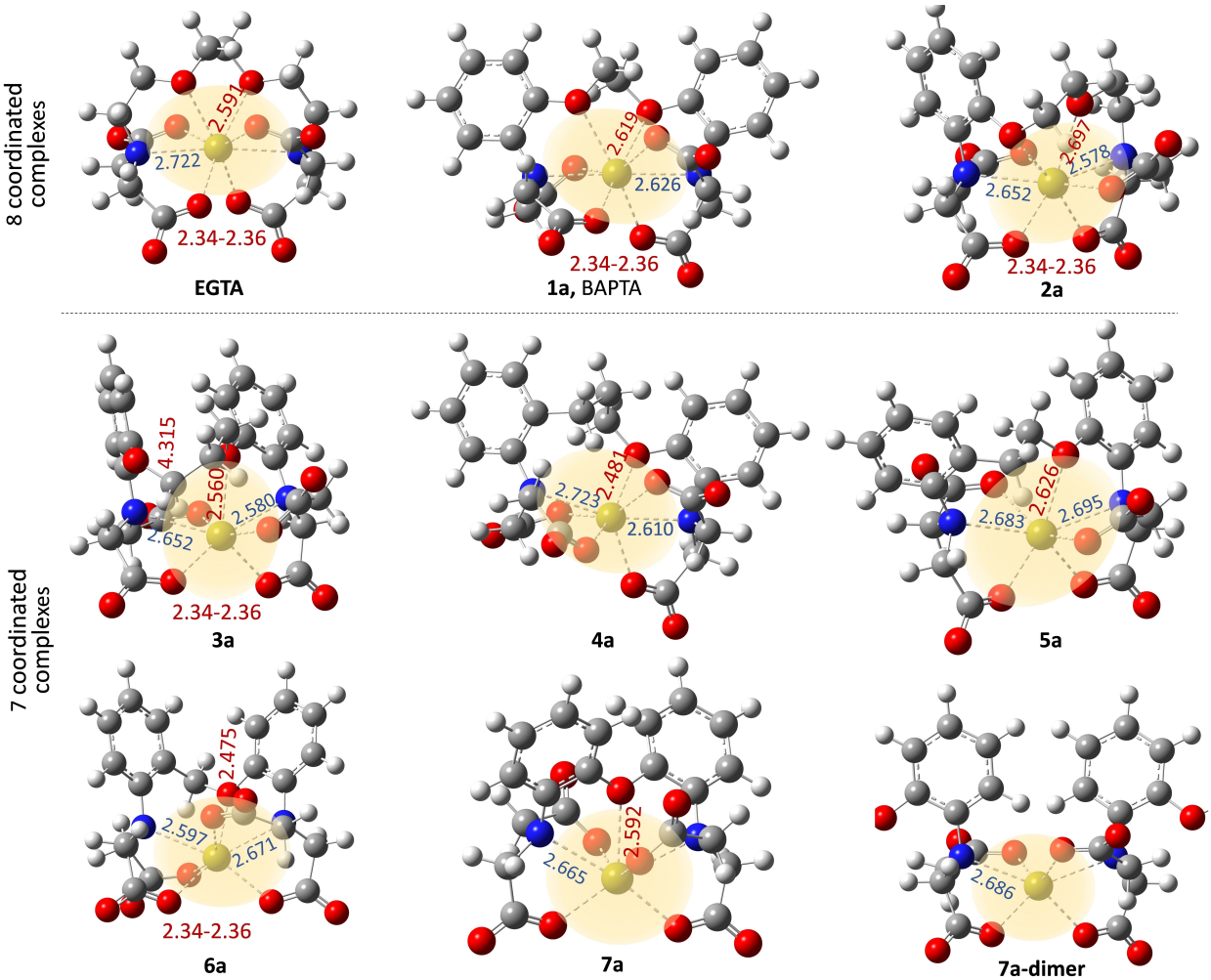

Figure 6. Optimized structures of the ionophores EGTA and **1a**–**7a** in the presence of Ca^{2+} calculated at M062X/6-31G(d,p) level of theory. For **7a**, two types of complex formation were considered, such as **7a** and **7a**-dimer, where the dimeric structure was modelled by one of the two Ca^{2+} centers surrounded by the coordinating donor atoms from two ligands. C–N and C–O bond lengths are given in blue and red numbers (in Ångstrom units), respectively. For details, see Table S1 in the supporting information. Binding cavities are illustrated by orange clouds.

atom is responsible mainly for the difference in the affinity of EGTA and BAPTA towards Ca^{2+}. In conclusion, an optimal chain length between the aromatic rings, an exact cavity volume and advantageous dynamic characteristics are present in BAPTA, which explains its effectiveness in calcium binding. These features are similarly present in the fluorescent derivative of AATA developed in this work. Moreover, the steep Ca^{2+}-induced fluorescence turn-on step observed for **7b** (ODATA) is expected to be the most useful feature in neurobiological diagnostic applications in which the detection of cellular signals with a large contrast is demanded. According to the computational results, we raise the possibility of the existence of a unique binding model, i.e., the formation of a dimeric complex, in this latter chelator. This study not only contributes to the clarification of why BAPTA currently performs so well in Ca^{2+} capture, but also opens up new possibilities for further structural optimizations that target specific sensing applications.

Experimental Section

Reagents and solvents were purchased from Sigma Aldrich in reagent grade and used as received, while NMR solvents were purchased from Eurisotop. Thin layer chromatography (TLC) was performed on commercially available pre-coated TLC plates (Merck Silica gel 60 F_{254} aluminium sheets or Merck Aluminium oxide 60 F_{254} plates). Visualisation was either achieved under UV light at 254 nm or by exposing the plates to iodine or to the aqueous solution of $(NH_4)_6Mo_7O_{24}$, $Ce(SO_4)_2$ and sulphuric acid. Melting points were determined on a Büchi M-560 capillary melting point apparatus and are uncorrected. For flash column chromatography an Interchim PuriFlash XS 420 system was employed using gradient elution on normal phase (silica or aluminium oxide column; hexane – EtOAc or DCM/MeOH as eluents). Preparative HPLC was applied for purification in many cases using an Armen SPOT Prep II instrument with UV detector (200–600 nm scan) equipped with a Phenomenex Gemini C18, 250×50.00 mm; 10 μm, 110 A column. Gradient elution was employed using 0.4 g NH_4HCO_3 in 1 L water (A) and acetonitrile (B) or 10 mL TFA in 1 L water (A) and acetonitrile (B) as eluent systems. NMR spectra were recorded on Varian Unity INOVA spectrometers operating at an equivalent ^1H

frequency of 400 and 500 MHz. Notations for the ^{1}H NMR spectral splitting patterns include singlet (s), doublet (d), triplet (t), broad (br) and multiplet/overlapping peaks (m). Chemical shifts of the resonances are given as δ values in ppm and coupling constants (*J*) are expressed in Hertz. Individual resonances were assigned on the basis of DEPT 135, 1D (NOESY) and 2D NMR (COSY, HSQC and HMBC) experiments. HRMS spectra were recorded on a Q Exactive Plus hybrid quadrupole-orbitrap mass spectrometer (Thermo Scientific, Waltham, MA, USA) equipped with a heated electrospray ionization (HESI-II) probe that was used in positive and negative ion mode. Samples were introduced with FIA (flow injection analysis) method and the eluent stream (water and acetonitrile in a 1:1 volume ratio with 0.1% formic acid) was provided by a Waters UPLC (Waters, Milford, USA).

UV/Vis absorption spectra were recorded were recorded on a Thermo Scientific Evolution 220 spectrometer in the wavelength range of 220–700 nm using a quartz cuvette (pathlength = 5.0 cm). The general sample preparation protocol involved the dissolution of 1–3 mg of the studied compounds in 10.0–15.0 mL of MOPS buffer (c = 0.03 M, pH = 7.2) that were diluted further to the concentrations used for the fluorescence Ca^{2+}-titrations by 'Buffer A' or 'Buffer B' (typically to $c_{dye} < 1.0$ μM). 'Buffer A' and 'Buffer B' are solutions containing the pH-buffer MOPS (c = 0.03 M), KCl background electrolyte (c = 0.1 M) and the Ca^{2+}-buffer EGTA (c = 0.01 M), adjusted to a pH value of 7.2. Besides these components, 'Buffer B' contains Ca^{2+} ions ($CaCl_2$) in a concentration identical to that of EGTA (c = 0.01 M). These background-corrected spectra of the relevant buffers ('Buffer A' or 'Buffer B') were subtracted from the sample spectra. These background-corrected spectra were used for determining the wavelength of absorption maxima (λ_{abs}) and the absorbances normalized to 1.0 M concentrations of the dyes (ε). Fluorescence emission spectra were acquired on a Hitachi F-4500 fluorescence spectrophotometer using a quartz cell (pathlength = 1.0 cm). Slit widths were selected to provide 2.5 nm bandpass both for the excitation and emission beams. Emission data were normalized to the intensity of an external reference probe body, recorded every day. Background emission spectra of the relevant buffers ('Buffer A' or 'Buffer B') were subtracted from the spectra of samples. Samples were excited at the wavelength values of their absorption maxima (λ_{abs}) determined during UV/fVis absorption measurements. Quantum yields were calculated by method published earlier.[20]

Fluorescence-monitored Ca2+-titrations were executed by using a solution of the selected dye molecule containing the Ca2+-buffer EGTA in a concentration of 0.01 M but no Ca2+ ions. These starting solutions were made by the dilution of the stock solution of the dye into 'Buffer A'. Another solution, containing the dye in the same concentration, was also prepared by using 'Buffer B'. This latter solution contained the Ca2+-buffer EGTA and Ca2+ ions at identical, 0.01 M concentration, setting the free Ca2+-level to 37 μ M. For the measurement of the first (0) point of the titration curve 2.0 mL of the sample made with 'Buffer A' was used. In the titration process various (typically increasing) volume fractions of the sample were replaced by the same volumes of the solution made with 'Buffer B'. Fine details of this fluorescence titration protocol have been described previously.[21,22]

Density-functional theory (DFT) computation was performed with the Gaussian 16 program package (G16),[24] using convergence criteria of 3.0×10^{-4}, 4.5×10^{-4}, 1.2×10^{-3} and 1.8×10^{-3}, for the gradients of the root mean square (RMS) force, maximum force, RMS displacement, and maximum displacement vectors, respectively. Computation was carried out at M062X/6 31G(d,p) level of theory.[25] The vibrational frequencies were computed at the same levels of theory, as used for geometry optimization, in order to properly confirm that all structures reside at minima on their potential energy hypersurfaces (PESs). Thermodynamic functions, such as energy (*U*), enthalpy (*H*), Gibbs free energy (*G*), and entropy (*S*) were computed for 298.15 K, using the quantum chemical, rather than the conventional thermodynamic reference state.

Synthesis and characterization

General procedure 1 for reduction. The nitro compound was suspended in EtOH and 5% of Pd/C (10 w/w % Pd in carbon) was added to the suspension. The mixture was flushed with argon in an autoclave, then filled with H_2 (10 bar pressure) and stirred overnight at room temperature. The suspension turned into yellow, it was filtered and concentrated *in vacuo* to yield the desired product, which was used in the next step without further purification.

General procedure 2 for N-alkylation. 27 mmol of the amino compound was dissolved in 20 ml MeCN, then Na_2HPO_4 (23 g, 162 mmol, 6 equiv.), KI (450 mg, 2.7 mmol, 0.1 equiv.) and 17.9 ml ethyl bromoacetate (27 g, 162 mmol, 6 equiv.) were added to the reaction mixture before stirring at 90 °C for 10–18 hours. The complete conversion to the tetraalkyl derivative was assured and confirmed by HPLC-MS, since the removal of underalkylated derivatives is difficult. The solvent was removed under reduced pressure. The resulting solids were dissolved in 150 ml water and 100 ml EtOAc was added. The layers were separated, and the aqueous phase was washed with 2×100 ml EtOAc. The combined organic phases were washed with water, then with brine and dried over $MgSO_4$. The solvent was removed under reduced pressure and the resulting oil was suspended in hexane, then cooled to 5 °C. The pure product precipitated as brownish crystals. If the crystallization did not occur (**11**, **14**), flash chromatography was used for purification on silica gel using a gradient elution (0% → 20% EtOAc in hexane). For compound **11**, the quantity of ethyl bromoacetate and the base was halved.

General procedure 3 for formylation.[19] 2 mmol of the ethyl esters in 5 ml DMF were added to a cool (0 °C) solution of $POCl_3$ (1.1 mmol, 100 μL, 1.1 equiv.) in 10 ml DMF. After stirring at room temperature for 2 hours, the mixture was neutralized by the addition of 10 w/w % aqueous solution of $NaHCO_3$. The organic compounds were extracted with EtOAc, the organic layers were combined, and the solvent was removed under reduced pressure. The product was purified using preparative HPLC.

General procedure 4 for coupling to the fluorophore.[16] Formylated compound (1 mmol, ca. 500 mg) was dissolved in 5 ml propionic acid and 3-diethylaminophenol (363,5 mg, 2.2 mmol, 2.2 equiv.) was added to the mixture. This solution was stirred under microwave irradiation in a sealed tube at 80 °C for 2–4 hours, then cooled to room temperature. A suspension of chloranil (233 mg, 0.95 mmol, 0.95 equiv.) in 5 ml DCM/EtOH 1:1 was added to the reaction mixture, and it was stirred at room temperature for overnight to promote the oxidative ring closure. The reaction mixture was concentrated and purified by preparative HPLC to afford the desired product.

General procedure 5 for hydrolysis of the ethyl esters. Ethyl ester (0.1 mmol) was dissolved in 5 ml EtOH and 20 w/w% NaOH solution (200 mg, ca. 200 μl, 1 mmol, 10 equiv.) was added to the solution and stirred for 20 minutes at room temperature. The reaction mixture was injected to preparative HPLC. The collected fractions were lyophilized to yield the desired final products.

Preparation of the fluorescent derivatives 1 b and 3 b (See Figure S1 in Supplementary Information)

The synthesis of BAPTA ethyl ester (**21**) and BAPPTA ethyl ester (**22**) were carried out following the procedure described in references[2,11] with minor modifications. K_2CO_3 (7.3 g, 53 mmol, 1.5 equiv.) was suspended in 40 ml DMF and a solution of 2-nitrophenol (4.9 g, 35.3 mmol, 1.0 equiv.) in 10 ml DMF was added under stirring. To this red solution 8.8 ml (15.2 g, 106.5 mmol, 3.0 equiv.) of 1-bromo-2-chloroethane was added in the case of BAPTA ethyl ester (**21**), while 9.8 ml (16.8 g, 106.5 mmol, 3 equiv.) of 1-bromo-2-chloropropane in the case of BAPPTA ethyl ester (**22**). 880 mg (5.3 mmol, 0.1 equiv.) of KI was added to each mixture and the solutions were stirred at 90 °C for 3 hours, then the solvents were removed under reduced pressure and the solid residues were dissolved in EtOAc and extracted with saturated Na_2CO_3, then with brine. The organic phase fractions were dried over $MgSO_4$, then the solvent was removed under reduced pressure. The resulting brown oil was dissolved in 30 ml DMF containing 7.3 g of suspended K_2CO_3 (53 mmol, 1.5 equiv.). 880 mg (5.3 mmol, 0.1 equiv.) of KI and 4.9 g 2-nitrophenol (35.3 mmol, 1 equiv.) was added and the mixture was stirred at 110 °C for 2 hours. The brownish mixture was poured on crushed ice. The white precipitate was filtered from the orange mother liqueur and washed with water, then dried overnight. Carrying out the reaction in two steps resulted in higher product purity. The products 1,2-bis(2-nitrophenoxy)ethane (**S2**) (beige powder, yield: 9.66 g, 90 %, melting point: 158 °C, ref 167 °C), and 1,2-bis(2-nitrophenoxy)propane (**S5**) (beige powder, yield: 14.4 g, 90 %, melting point: 108 °C, ref 106 °C) were used without further purification.

Hydrogenations were carried out under pressure (10 bar), compared to the previous methods,[2] using *general procedure 1*. described in *S3.1.1*. starting from the quantities from the quantity given above. The products 1,2-bis(2-aminophenoxy)ethane (**S3**) (yield: 7.13 g, 92 %) and 1,2-bis(2-aminophenoxy)propane (**S6**) (yield: 10.72 g, 94 %) were isolated as yellow oils.

Alkylations were performed based on *general procedure 2*, starting from 6.58 g and 6.96 g of amine. The Ethyl ester products **21** (yield: 14.45 g, 91 %, melting point: 99 °C, ref 95–97 °C) and **22** (yield: 14.62 g, 90 %, melting point: 77 °C, ref 76 °C) were isolated as brown crystals. The spectroscopic properties of all above compounds are in agreement with previously published data.[2,11]

The formylations were performed according to *general procedure 3* from 1 mmol of starting materials. The aldehyde compounds **24** (yield: 262 mg, 42.5 %, melting point: 109 °C; ref 139 °C.) and **26** (yield: 296 mg, 47 %, melting point: 83 °C.) were isolated as brown solids. The spectroscopic properties of compound **24** are in agreement with data previously reported.[19] The spectroscopic properties of compound **26**: ^{1}H NMR (400 MHz, [D$_6$]DMSO) δ = (s, 1H, C[32]–H), 7.39 (dd, *J* = 8.2, 1.8 Hz, 1H, C[3]–H), 7.33 (d, *J* = 1.9 Hz, 1H, C[5]–H), 6.89 (dd, *J* = 7.8, 1.9 Hz, 1H, C[14]–H), 6.85–6.76 (dt, *J* = 14.9, 7.3, 1.8 Hz, 2H, C[12–13]–H), 6.71–6.65 (m, 2H, C[2, 11]–H), 4.19 (s, 4H, C[16–17]–H), 4.12–4.02 (m, 16H, C[7,9,18–19,20–23]–H), 2.05 (t, *J* = 6.2 Hz, 2H, C[8]–H), 1.15 (dt, *J* = 14.1, 7.1 Hz, 12H, C[24–27]–H). ^{13}C {^{1}H} NMR (101 MHz, [D$_6$]DMSO) δ = 190.7, 170.8, 170.3, 149.7, 148.7, 144.5, 138.7, 128.8, 125.5, 121.3, 120.8, 118.1, 115.9, 113.2, 111.4, 65.5, 65.1, 60.4, 60.1, 53.7, 53.3, 28.5, 14.1. HRMS (ESI +): *m/z* calcd for $C_{32}H_{43}N_2O_{11}^+$ ([M + H]$^+$): 631.28614, found: 631.28611.

The couplings to the fluorophores were carried out using the *general procedure 4* using the quantities given above. The tetraethyl ester compounds **31** (yield: 119 mg, 20 %, melting point: decomposed) and **33** (yield: 205 mg, 22 %, melting point: decomposed) were isolated as red powders.

The spectroscopic properties of compound **31**: ^{1}H NMR (400 MHz, [D$_6$]DMSO) δ = 7.46 (d, J = 9.6 Hz, 2H, C[33, 42]–H), 7.16–7.09 (m, 3H, C[5, 34, 41]–H), 7.03 (dd, J = 8.2, 1.9 Hz, 1H, C[3]–H), 6.94 (dd, J = 15.3, 2.2 Hz, 3H, C[13, 36, 39]–H), 6.89–6.81 (m, 3H, C[2, 11–12]–H), 6.68 (dd, J = 7.3, 2.3 Hz, 1H, C[10]–H), 4.26–4.13 (m, 8H, C[7–8, 15–16]–H), 4.06 (s, 4H, C[17–18]–H), 3.96 (dq, J = 21.7, 7.1 Hz, 8H, C[44–47]–H), 3.67 (s, 8H, C[19–22]–H), 1.21 (t, J = 7.0 Hz, 12H, C[48–51]–H), 1.06 (td, J = 7.1, 5.3 Hz, 12H, C[23–26]–H). ^{13}C {^{1}H} NMR (101 MHz, [D$_6$]DMSO) δ = 170.8, 170.7, 157.4, 156.8, 154.9, 149.5, 148.8, 140.7, 138.8, 132.0, 123.4, 123.3, 121.3, 121.1, 117.9, 116.9, 114.8, 114.2, 113.1, 112.6, 96.0, 67.5, 66.8, 60.4, 60.1, 53.3, 53.1, 45.3, 13.9, 13.9, 12.5. HRMS (ESI +): *m/z* calcd for $C_{51}H_{65}N_4O_{11}^+$ ([M]$^+$): 909.46444, found: 909.46217.

The spectroscopic properties of compound **33**: ^{1}H NMR (400 MHz, [D$_6$]DMSO) δ = 7.48 (d, J = 9.6 Hz, 2H, C[24, 43]–H), 7.16–7.05 (m, 3H, C[5, 35, 42]–H), 6.97 (dd, J = 19.3, 5.2 Hz, 3H, C[2, 37, 40]–H), 6.89–6.83 (m, 2H, C[3, 14]–H), 6.77 (dt, J = 13.9, 7.0 Hz, 2H, C[12, 13]–H), 6.61 (dd, J = 7.6, 2.1 Hz, 1H, C[11]–H), 4.23 (s, 4H, C[16–17]–H), 4.18–3.93 (m, 16H, C[7, 9, 18–19, 20–23]–H), 3.64 (d, J = 7.1 Hz, 8H, C[45–48]–H), 2.05 (p, J = 6.2 Hz, 2H, C[8]–H), 1.21 (td, J = 7.0, 4.4 Hz, 18H, C[24–25, 49–52]–H), 1.09 (t, J = 7.1 Hz, 6H, C[26–27]–H). ^{13}C {^{1}H} NMR (101 MHz, [D$_6$]DMSO) δ = 170.9, 170.7, 158.2, 157.9, 157.4, 156.8, 154.9, 149.5, 148.8, 140.6, 138.6, 132.1, 123.3, 121.3, 120.8, 117.9, 114.7, 114.2, 113.0, 112.5, 104.6, 96.0, 65.7, 60.4, 60.1, 53.5, 53.2, 45.3, 28.6, 14.2, 14.1, 12.5. HRMS (ESI +): *m/z* calcd for $C_{52}H_{67}N_4O_{11}^+$ ([M]$^+$): 923.48009, found: 923.47866.

The hydrolysis of the ethyl esters were carried out using the *general procedure 5.* using the quantities given above. The fluorescent dyes **1 b** (red powder, yield: 38 mg, 62 %, melting point: decomposed at > 110 °C.) and **3 b** (yield: 52 mg, 85 %, melting point: decomposed at 116 °C.) were isolated as red powders. The spectroscopic properties of compound **1 b**: ^{1}H NMR (400 MHz, [D$_6$]DMSO) δ = 12.55 (bs, 4H, C[19–22]OO–H), 7.50 (d, J = 8.2 Hz, 2H, C[25, 34]–H), 7.19 (d, J = 1.9 Hz, 1H, C[5]–H), 7.16 (dd, J = 8.2, 2.2 Hz, 2H, C[26, 33]–H), 7.11–6.72 (m, 8H, C[2, 3, 10–13, 28, 31]–H), 4.31 (t, J = 7.0 Hz, 4H, C[7, 8]–H), 4.24 (s, 4H, C[15–16]–H), 4.02 (s, 4H, C[17–18]–H), 3.96 (q, J = 7.1 Hz, 8H, C[36–39]–H), 1.20 (t, 12H, J = 7.0 Hz, C[19–22]–H). ^{13}C {^{1}H} NMR (101 MHz, [D$_6$]DMSO) δ = 172.5, 172.3, 157.4, 156.7, 154.9, 149.4, 148.4, 141.3, 139.3, 132.2, 123.9, 122.8, 121.5, 121.1, 118.2, 116.8. 116.1, 114.8, 114.2, 112.5. 96.0, 67.5, 67.0, 53.7, 53.5, 45.3, 12.5. HRMS (ESI +): *m/z* calcd for $C_{43}H_{49}N_4O_{11}^+$ ([M]$^+$): 797.33923, found: 797.33812.

The spectroscopic properties of compound **3 b**: ^{1}H NMR (400 MHz, [D$_6$]DMSO) δ = 12.55 (s, 4H, C[20–23]OO–H), 7.49 (d, J = 9.6 Hz, 2H, C[26, 35]–H), 7.11 (dd, J = 9.6, 2.5 Hz, 2H, C[27, 34]–H), 7.06 (d, J = 2.0 Hz, 1H, C[5]–H), 7.00 (dd, J = 8.2, 1.9 Hz, 1H, C[3]–H), 6.94 (d, J = 2.5 Hz, 2H, C[29, 32]–H), 6.91–6.86 (dd, J = 9.6, 2.5 Hz, 1H, C[14]–H), 6.83 (d, J = 8.3 Hz, 1H, C[2]–H), 6.76 (dt, J = 7.1, 6.4, 3.6 Hz, 2H, C[12–13]–H), 6.66–6.59 (m, 1H, C[11]–H), 4.16 (s, 4H, C[16–17]–H), 4.11 (t, J = 6.4 Hz, 2H, C[9]–H), 4.07 (t, J = 5.9 Hz, 2H, C[7]–H), 3.92 (s, 4H, C[18–19]–H), 3.64 (q, J = 7.0 Hz, 8H, C[37–40]–H), 2.19–2.10 (m, 2H, C[8]–H), 1.21 (t, J = 7.0 Hz, 12H, C[41–44]–H). ^{13}C {^{1}H} NMR (101 MHz, [D$_6$]DMSO) δ = 172.6, 172.3, 157.4, 156.8, 154.8, 149.5, 148.7, 141.0, 138.9, 132.1, 123.4, 122.8, 120.9, 120.7, 117.5, 116.4, 114.7, 114.2, 113.0, 112.4, 95.9, 65.7, 64.9, 53.6, 53.4, 45.2, 28.7, 12.5. HRMS (ESI +): *m/z* calcd for $C_{44}H_{51}N_4O_{11}^+$ ([M]$^+$): 811.35488, found: 811.35354.

Preparation of the fluorescent dye 2 b. (See Figure S2 in Supplementary Information)2-nitrophenol (10 g, 72 mmol, 1.0 equiv.) was dissolved in DMF (150 ml), then K_2CO_3 (14.9 g, 108 mmol, 1.5 equiv.), and KI (1.19 g, 7.2 mmol, 0.1 equiv.) were added. The mixture was stirred at 110 °C, 2-chloroethyl ether (30.8 g, 25.3 ml, 216 mmol, 3.0 equiv.) was added and stirred for 2 hours at 110 °C. The solvents were removed under reduced pressure and the solid

residue was dissolved in EtOAc and water. The layers were separated, the organic phase was extracted with saturated aqueous Na_2CO_3 and brine. The mixture was dried over $MgSO_4$, the solvent was removed under reduced pressure. Mononitro compound **8** (brown oil, yield: 21.7 g, 92%) was used in the next step without further purification. The spectroscopic properties of **8** are in good agreement with those published previously.[26]

11.5 g (37.5 mmol, 1.0 equiv.) of **8** was dissolved in 100 ml DMF and 10.1 g DIPEA (77.9 mmol, 13.6 ml, 2.0 equiv.). 12. 8 g diethyl iminodiacetate (67.5 mmol, 12.1 ml, 1.8 equiv.) was added and the mixture was stirred at 120 °C for 2 days. Additional 7.09 g (37.5 mmol, 6. 7 ml, 1.0 equiv.) diethyl iminodiacetate and 2 g (12 mmol, 0,32 equiv.) of KI were added, then stirred for 4 days. The solvents were removed under reduced pressure, the solid residue was dissolved in EtOAc and the mixture was extracted with saturated aqueous Na_2CO_3, then with brine. The organic phase was dried over $MgSO_4$, then the solvent was removed under reduced pressure. Product **9** was isolated as a brown oil (yield: 21.8 g, 80%). ^{1}H NMR (400 MHz, [D$_6$]DMSO) δ = 7.86 (dd, J = 8.1, 1.7 Hz, 1H, C[2]–H), 7.64 (ddd, J = 8.8, 7.4, 1.7 Hz, 1H, C[3]–H), 7.37 (dd, J = 8.6, 1.1 Hz, 1H, C[5]–H), 7.12 (dt, J = 8.3, 7.4, 1.1 Hz, 1H, C[4]–H), 4.26 (t, J = 5.2 Hz, 2H, C[7]–H), 4.08 (q, J = 7.1 Hz, 4H, C[13–14]–H), 3.80 (s, 4H, C[11–12]–H), 3.76 (t, J = 5.2 Hz, 2H, C[8]–H), 3.67 (t, J = 5.2 Hz, 2H, C[9]–H), 3.10 (t, J = 5.2 Hz, 2H, C[10]–H), 1.16 (t, J = 7.1 Hz, 6H, C[15–16]–H). ^{13}C {^{1}H} NMR (101 MHz, [D$_6$]DMSO) δ = 169.1, 151.3, 139.6, 134.4, 125.0, 120.7, 115.3, 69.0, 68.5, 68.1, 60.6, 54.9, 53.7, 13.9. HRMS (ESI+): m/z calcd for $C_{18}H_{27}N_2O_8^+$ ([M+H]$^+$): 399.17620, found: 399.17621.

Reduction of **9** was carried out according to *general procedure 1* starting from 26 mmol of staring material. The amine compound **10** (yield: 9,3 g, 97%) was isolated as a brown oil. ^{1}H NMR (400 MHz, [D$_6$]DMSO) δ = 7.21–7.11 (m, 3H, C[2–3, 5]–H), 6.96 (dt, J = 8.3, 7.3, 1.1 Hz, 1H, C[4]–H), 4.17 (t, J = 5.2 Hz, 2H, C[7]–H), 4.08 (q, J = 7.1 Hz, 4H, C[13–14]–H), 3.74 (t, J = 5.5 Hz, 2H, C[8]–H), 3.69 (s, 4H, C[11–12]–H), 3.63 (t, J = 5.5 Hz, 2H, C[9]–H), 2.98 (t, J = 5.5 Hz, 2H, C[10]–H), 1.18 (t, J = 7.1 Hz, 6H, C[15–16]–H). ^{13}C {^{1}H} NMR (101 MHz, [D$_6$]DMSO) δ = 170.0, 150.2, 121.6, 121.3, 117.3, 114.4, 113.5, 68.8, 68.7, 68.3, 60.2, 55.1, 53.3, 14.0. HRMS (ESI+): m/z calcd for $C_{18}H_{29}N_2O_6^+$ ([M+H]$^+$): 369.20202, found: 369.20183.

Alkylation of **10** was carried out according to *general procedure 2*. starting from 9.3 mmol of starting compound to yield **11**. The quantity of ethyl bromoacetate was halved compared to other compounds. The ethyl ester compound **11** (yield: 3,5 g, 70%) was isolated as a brown oil. The spectroscopic properties of **11** are in good agreement with those published.[12] The formylation was performed according to *general procedure 3* starting from 2.5 mmol staring material. The aldehyde compound **25** (yield: 470 mg, 35%) was isolated as a brown viscous oil. ^{1}H NMR (400 MHz, [D$_6$]DMSO) δ = 9.75 (s, 1H, C[27]–H), 7.41 (dd, J = 8.3, 1.8 Hz, 1H, C[3]–H), 7.35 (d, J = 1.8 Hz, 1H, C[5]–H), 6.75 (d, J = 8.3 Hz, 1H, C[2]–H), 4.25 (s, 4H, C[11–12]–H), 4.17–4.02 (m, 10H, C[7, 15–18]–H), 3.67 (s, 6H, C[8, 13–14]–H), 3.59 (t, J = 5.6 Hz, 2H, C[9]–H), 2.98 (t, J = 5.5 Hz, 2H, C[10]–H), 1.18 (dt, J = 14.8, 7.1 Hz, 12H, C[19–22]–H). ^{13}C {^{1}H} NMR (101 MHz, [D$_6$]DMSO) δ = 190.4, 170.0, 169.9, 148.6, 144.4, 128.7, 125.3, 116.1, 112.4, 68.6, 68.3, 67.9, 60.2, 60.0, 55.0, 53.7, 53.4, 13.9, 13.9. HRMS (ESI+): m/z calcd for $C_{27}H_{41}N_2O_{11}^+$ ([M+H]$^+$): 569.27049, found: 569.27001.

The coupling to the fluorophore was carried out using the *general procedure 4* starting from 0.6 mmol of formyl compound. The tetraethyl ester compound **32** (yield: 80 mg, 15%) was isolated as blue crystals. Melting point: decomposed at > 145 °C. ^{1}H NMR (400 MHz, [D$_6$]DMSO) δ = 7.47 (d, J = 9.6 Hz, 2H, C[29, 38]–H), 7.20–7.06 (m, 3H, C[5, 30, 37]–H), 7.01 (dd, J = 8.2, 1.9 Hz, 1H, C[2]–H), 6.94 (d, J = 2.5 Hz, 2H, C[32, 35]–H), 6.92 (d, J = 8.2 Hz, 1H, C[3]–H), 4.27 (s, 4H, C[11–12]–H), 4.16 (q, J = 7.1 Hz, 4H, C[15–16]–H), 4.09 (t, J = 5.8 Hz, 2H, C[7]–H), 4.03 (q, J = 7.1 Hz, 4H, C[17–18]–H), 3.66 (m, 10H, C[8, 40–43]–H), 3.54 (t, J = 5.8 Hz, 2H, C[9]–H), 3.51 (s, 4H, C[13–14]–H), 2.85 (t, J = 5.8 Hz, 2H, C[10]–H), 1.23 (t, J = 7.2 Hz,18H, C[19–20, 44–47]–H), 1.14 (t, J = 7.1 Hz, 6H, C[21–22]). ^{13}C {^{1}H} NMR (101 MHz, [D$_6$]DMSO) δ = 170.5, 170.2, 164.1, 157.3, 154.8, 148.8, 140.6, 131.8, 123.2, 117.2, 115.8, 114.1, 112.4, 95.9, 69.3, 68.4, 68.2, 60.0, 59.5, 55.0, 53.4, 53.0, 45.1, 44.7, 13.9, 13.8, 12.2. HRMS (ESI+): m/z calcd for $C_{47}H_{65}N_4O_{11}^+$ ([M]$^+$): 861.46444, found: 861.46278.

The hydrolysis of this ethyl ester was carried out using the *General procedure 5* staring from the quantity given above. The fluorescent dye **2b** (yield: 19 mg, 64%) was isolated as blue crystals. Melting point: decomposed at > 110 °C. ^{1}H NMR (400 MHz, [D$_6$]DMSO) δ = 7.49 (d, J = 9.6 Hz, 2H, C[21, 30]–H), 7.14 (dd, J = 9.6, 2.4 Hz, 2H, C[22, 29]–H), 7.09 (d, J = 2.0 Hz, 1H, C[5]–H), 7.02 (d, J = 8.3 Hz, 1H, C[2]), 6.95 (d, J = 2.4 Hz, 2H, C[24, 27]–H), 6.85 (d, J = 8.3 Hz, 1H, C[3]–H), 4.18 (s, 4H, C[11–12]–H), 4.07 (t, J = 4.5 Hz, 2H, C[7]–H), 3.82 (s, 4H, C[13–14]–H), 3.66 (m, 12H, C[8–9, 32–35]–H), 3.18 (s, 2H, C[10]–Hf), 1.21 (t, J = 7.0 Hz, 12H, C[36–39]–H). ^{13}C {^{1}H} NMR (101 MHz, [D$_6$]DMSO) δ = 172.2, 170.1, 157.4, 156.8, 154.9, 148.5, 141.0, 132.1, 123.6, 122.7, 116.6, 115.3, 114.2, 112.5, 96.0, 68.6, 68.0, 55.0, 54.3, 53.6, 45.3, 36.5, 12.5. HRMS (ESI+): m/z calcd for $C_{39}H_{49}N_4O_{11}^+$ ([M]$^+$): 749.33923, found: 749.33765.

Preparation of the fluorescent dye 4b

To perform the initial alkylation shown in Scheme 2, 2-nitrophenol (10 g, 72 mmol, 1.0 equiv.) was dissolved in dry DMF (20 ml), then K_2CO_3 (19.9 g, 144 mmol, 2.0 equiv.) was added. The mixture was stirred at 110 °C for 2 hours after the addition of (3-bromopropyl) benzene (15.8 g, 11.7 ml, 79.2 mmol, 1.1 equiv.). The formed solids were filtered out. Mononitro compound **12** (yield: 17.4 g, 94%) was isolated as brown oil. The spectroscopic properties of the compound are in good agreement with the ones reported in the literature.[27]

To achieve precursor **13**, 9.5 g of **12** (37 mmol, 1.0 equiv.) was dissolved in 30 ml 65% HNO_3 (7.5 equiv.) and 1 ml of conc. H_2SO_4 was added. The mixture was stirred at 110 °C for 1 hour, then poured on 100 ml icy water. The aqueous phase was extracted with 3x50 ml EtOAc. The organic layer was washed with 30 ml of saturated aqueous Na_2CO_3, then washed with brine, dried over $MgSO_4$ and concentrated to give 9.1 g of yellow oil. The reduction step was carried out according to *general procedure 1*. starting from the mixture of isomers present in the crude product. The isomers were separated at the end of reduction by preparative HPLC. The amine compound **13** (yield: 3.13 g, 35% for the overall process) was isolated as an off-white powder. Melting point: 183 °C. ^{1}H NMR (400 MHz, [D$_6$]DMSO) δ = 7.24–6.91 (m, 8H, C[2–5, 11–14]–H), 4.07 (t, J = 6.1 Hz, 2H, C[7]–H), 2.77 (t, J = 6.1 Hz, 2H, C[9]–H), 2.03 (q, J = 7.9 Hz, 2H, C[8]–H). ^{13}C {^{1}H} NMR (100 MHz, [D$_6$]DMSO) δ = 150.1, 137.4, 130.2, 130.0, 127.2, 126.0, 125.1, 123.1, 121.3, 120.9, 119.7, 112.6, 67.6, 28.6, 26.4. HRMS (ESI+): m/z calcd for $C_{15}H_{19}N_2O^+$ ([M+H]$^+$): 243.14919, found: 243.14890.

Alkylation of **13** was carried out according to *general procedure 2*. from 4 mmol of amine to yield **14**. The ethyl ester compound **14** (yield: 0.94 g, 40%) was isolated as brown crystals. ^{1}H NMR (400 MHz, [D$_6$]DMSO) δ = 7.25–7.15 (m, 2H, C[11, 14]–H), 7.12 (td, J = 7.6, 1.7 Hz, 1H, C[13]–H), 7,02 (td, J = 7.5, 1.6 Hz, 1H, C[12]–H), 6.91–6.76 (m, 3H, [3–5]–H), 6.69 (dd, J = 7.2, 2.3 Hz, 1H, [2]–H), 4.18–3.90 (m, 18H, C[7, 16–23]–H), 2.78 (t, J = 7.9 Hz, 2H, C[9]–H), 2.02 (t, J = 11.1 Hz, 2H, C[8]–H), 1.20–1.08 (m, 14H, C[24–27]–H). ^{13}C {^{1}H} NMR (101 MHz, [D$_6$]DMSO) δ = 170.8, 170.5, 170.3, 149.9, 148.3, 138.6, 136.9, 129.4, 126.3, 124.2, 123.2, 121.3, 120.7, 118.2, 113.3, 68.2, 60.1, 60.0, 54.9, 54.4, 53.4, 29.2, 26.9, 14.1, 14.1, 14.0. HRMS

(ESI+): *m/z* calcd for $C_{31}H_{43}N_2O_9^+$ ([M+H]$^+$): 587.29631, found: 587.29669.

The formylation was performed according to *general procedure 3* from the quantity given above. The aldehyde compound **27** (yield: 350 mg, 28%) was isolated as brown crystals. ^{1}H NMR (400 MHz, [D$_6$]DMSO) δ=9.73 (s, 1H, C[32]–H), 7.39 (dd, J=8.3, 1.8 Hz, 1H, C[3]–H), 7.31 (d, J=1.8 Hz, 1H, C[5]–H), 7.20 (td, J=6.1, 5.7, 3.1 Hz, 2H, C[11, 14]–H), 7.12 (td, J=7.6, 1.7 Hz, 1H, C[13]–H), 7.02 (td, J=7.6, 1.7 Hz, 1H, C[12]–H), 6.70 (d, J=8.3 Hz, 1H, C[2]–H), 4.23 (s, 4H, C[16–17]–H), 4.13–3.87 (m, 14H, C[7, 18–19, 20–23]–H), 2.77 (t, J=7.7 Hz, 2H, C[9]–H), 2.04 (t, J=7.7 Hz, 2H, C[8]–H), 1.12 (dt, J=16.2, 7.1 Hz, 12H, C[24–27]–H). ^{13}C {^{1}H} NMR (101 MHz, [D$_6$]DMSO) δ=190.7, 170.3, 170.3, 148.8, 148.3, 144.5, 136.7, 129.3, 128.8, 126.4, 125.3, 124.2, 123.2, 115.9, 111.6, 68.5, 60.4, 60.1, 54.9, 53.8, 28.8, 26.7, 14.0. HRMS (ESI+): *m/z* calcd for $C_{32}H_{43}N_2O_{10}^+$ ([M+H]$^+$): 615.29123, found: 615.29158.

The coupling to the fluorophore was carried out using the *general procedure 4* from the quantity given above. The tetraethyl ester compound **34** (yield: 75 mg, 15%) was isolated as purple powder. Melting point: decomposed at >120 °C. ^{1}H NMR (400 MHz, [D$_6$]DMSO) δ=7.45 (d, J=9.5 Hz, 2H, C[34, 43]–H), 7.28–6.91 (m, 10H, C[3, 5, 11–14, 35, 37, 40, 42]–H), 6.86 (d, J=8.3 Hz, 1H, C[2]–H), 4.25 (s, 4H, C[16–17]–H), 4.12 (q, J=7.2 Hz, 4H, C[20–21]–H), 3,98–3.88 (m, 10H, C[7, 18–19, 22–23]–H), 3.65 (q, J=7.2 Hz, 8H, C[45–48]–H), 2.75 (t, J=7.6 Hz, 2H, C[9]–H), 2.04 (d, J=9.4 Hz, 2H, C[8]–H), 1.24–1.03 (m, 24H, C[24–27, 49–52]–H). ^{13}C {^{1}H} NMR (101 MHz, CDCl$_3$) δ=171.3, 171.0, 158.2, 157.9, 155.4, 150.2, 148.8, 141.3, 137.1, 132.5, 129.5, 126.8, 125.0, 124.4, 124.4, 123.2, 117.8, 114.3, 113.8, 113.4, 96.7, 69.0, 61.2, 60.7, 55.0, 53.9, 46.2, 29.4, 27.1, 14.4, 14.3, 12.7. HRMS (ESI+): *m/z* calcd for $C_{52}H_{67}N_4O_{10}^+$ ([M+H]$^+$): 907.48517, found: 907.48551.

The hydrolysis was carried out using the *general procedure 5* from the quantity given above. The fluorescent dye **4b** (yield: 20 mg, 54%) was isolated as purple powder. Melting point: decomposed at >100 °C. ^{1}H NMR (400 MHz, [D$_6$]DMSO) δ=12.68 (bs, 4H, C[20–23]OO–H), 7.48 (d, J=9.5 Hz, 2H, C[26, 35]–H), 7.23–6.91 (m, 10H, C[3, 5, 11–14, 27, 29, 32, 34]–H), 6.84 (d, J=8.2 Hz, 1H, C[2]–H), 4.19 (s, 4H, C[16–17]–H), 3.97 (t, J=6.5 Hz, 2H, C[7]–H), 3.85 (s, 4H, C[18–19]–H), 3.64 (q, J=7.2 Hz, 8H, C[37–40]–H), 2.76 (t, J=7.9 Hz, 2H, C[9]–H), 2.08 (s, 2H, C[8]–H), 1.21 (t, J=7.0 Hz, 12H, C[41–44]–H). ^{13}C {^{1}H} NMR (101 MHz, [D$_6$]DMSO) δ=172.3, 172.0, 157.4, 156.8, 154.8, 148.8, 148.7, 140.9, 136.4, 132.2, 129.8, 128.2, 126.2, 123.9, 123.6, 122.9, 122.8, 114.9, 114.2, 112.5, 96.0, 68.5, 54.6, 53.7, 45.3, 29.0, 26.9, 12.5. HRMS (ESI+): *m/z* calcd for $C_{44}H_{51}N_4O_{10}^+$ ([M]$^+$): 795.35997, found: 795.35955.

Preparation of the fluorescent dye 5b

5 g (36 mmol, 1.0 equiv.) 2-nitrophenol was suspended in 70 ml abs. THF, then the solution was cooled to 0 °C and stored under argon. 10.37 g (40 mmol, 1.1 equiv.) triphenylphosphine and 7.75 ml (8 g, 40 mmol, 1.1 equiv.) of DIAD were added. The suspension was let to warm up to room temperature for an hour. After this step it was cooled to 0 °C again, then 5 ml (6 g, 36 mmol, 1.0 equiv.) of 2-nitro-phenethyl-alcohol in 5 ml THF was added dropwise into the solution. After stirring for 12 hours at room temperature, the solvent was removed under reduced pressure, and the solid residue was dissolved in 70 ml DCM and extracted with 2x 40 ml 10% NaOH solution, then with brine. The organic phase fractions were dried over Na_2SO_4, then the solvent was removed under reduced pressure. The formed yellow oil was purified with flash chromatography on a silica column with Hexane: EtOAc=10:3 eluent. The resulting fractions were combined, and the solvent was removed under reduced pressure. The nitro compound **15** (yield: 8.54 g, 83%) was isolated as white crystals. Melting point: 99 °C. ^{1}H NMR (400 MHz, [D$_6$]DMSO) δ=7.98 (dd, J=8.1, 1.4 Hz, 1H, C[13]–H), 7.84 (dd, J=8.0, 1.7 Hz, 1H, C[2]–H), 7.72–7.57 (m, 3H, C[4, 10, 12]–H), 7.52 (td, J=8.7, 7.4, 1.6 Hz, 1H, C[11]–H), 7.37 (dd, J=8.0, 1.5 Hz, 1H, C[5]–H), 7.11 (td, J=8.7, 7.4, 1.6 Hz, 1H, C[3]–H), 4.44 (t, J=6.4 Hz, 2H, C[7]–H), 3.32 (t, J=6.4 Hz, 2H, C[8]–H). ^{13}C {^{1}H} NMR (101 MHz, [D$_6$]DMSO) δ=150.9, 149.3, 139.5, 134.5, 133.3, 133.2, 132.3, 128.3, 125.0, 124.6, 120.8, 115.1, 68.7, 31.7. HRMS (ESI+): *m/z* calcd for $C_{14}H_{16}N_3O_5^+$ ([M+NH$_4$]$^+$): 306.10845, found: 306.10837.

The reduction step was carried out according to *general procedure 1*. starting from the quantities given above. The resulting yellow oil was dissolved in 90 ml EtOAc, and 50 ml water was added. The layers were separated, and the aqueous phase was extracted with 2x60 ml EtOAc, Then the united organic phase fractions were washed with brine, and the EtOAc was removed under reduced pressure. The resulting brownish oil still contained some DIAD, but after putting the oil into the fridge overnight, the product precipitated as crystals. The crystals were washed with water, filtered, then dried. The amine compound **16** (yield: 5,82 g, 87%) was isolated as a beige powder. Melting point: 71 °C.^{1}H NMR (400 MHz, [D$_6$]DMSO) δ=7.04 (dd, J=7.5 Hz, 1.6 Hz, 1H, C[10]–H), 6.93 (td, J=7.6, 1.6 Hz, 1H, C[12]–H), 6.76 (dd, J=8.0, 1.4 Hz, 1H, C[5]–H), 6.70–6.59 (m, 3H, C[2, 4, 11]–H), 6.56–6.46 (m, 2H, C[3, 13]–H), 4.81 (d, J=87.8 Hz, 4H, C[1, 14]N–H), 4.07 (t, J=6.6 Hz, 2H, C[7]–H), 2.95 (t, J=6.6 Hz, 2H, C[8]–H). ^{13}C {^{1}H} NMR (101 MHz, [D$_6$] DMSO) δ=146.7, 145.6, 137.8, 130.3, 127.1, 121.9, 121.0, 116.3, 116.3, 114.9, 113.8, 111.7, 67.3, 30.8. HRMS (ESI+): *m/z* calcd for $C_{14}H_{17}N_2O^+$ ([M+H]$^+$): 229.13354, found: 229.13332.

Alkylation of **16** was carried out according to *general procedure 2*. from 3 mmol of amine to yield **17**. The ethyl ester compound **17** (yield: 1.1 g, 63%) was isolated as a yellow oil. ^{1}H NMR (400 MHz, [D$_6$]DMSO) δ=7.31–7.23 (m, 2H, C[10, 13]–H), 7.15 (td, *J*=7.6, 1.7 Hz, 1H, C[12]–H), 7.02 (td, *J*=7.4, 1.3 Hz, 1H, C[11]–H), 6.91 (dd, *J*=7.6, 2.0 Hz, 1H, C[5]–H), 6.85–6.74 (m, 2H, C[3–4]–H), 6.69 (dd, *J*=7.4, 2.1 Hz, 2H, C[2]–H), 4.20 (t, *J*=7.4 Hz, 2H, C[7]–H), 4.09–3.95 (m, 16H,C[15–22]–H), 3.06 (t, *J*=7.4 Hz, 2H,C[8]–H), 1.11 (dt, *J*=20.6, 7.1 Hz, 12H, C[23–26]–H). ^{13}C {^{1}H} NMR (101 MHz, [D$_6$]DMSO) δ=170.8, 170.3, 149.8, 148.7, 138.6, 133.8, 130.4, 126.9, 124.5, 123.4, 121.4, 120.8, 118.3, 113.5, 68.1, 60.1, 60.1, 55.0, 53.4, 30.6, 14.1, 14.0. HRMS (ESI+): *m/z* calcd for $C_{30}H_{41}N_2O_9^+$ ([M+H]$^+$): 573.28066, found: 573.28038.

The formylation was performed according to *general procedure 3* starting from the quantities given above. The aldehyde compound **28** (yield: 985 mg, 82%) was isolated as a brown oil. ^{1}H NMR (400 MHz, [D$_6$]DMSO) δ=9.70 (s, 1H, C[31]–H), 7.38 (dd, J=4.3, 2.6 Hz, 2H, C[3, 5]–H), 7.26 (dd, J=8.0, 1.5 Hz, 2H, C[10, 13]–H), 7.16 (td, J=7.5, 1.7 Hz, 1H, C[12]–H), 7.03 (td, J=7.3, 1.3 Hz, 1H, C[11]–H), 6.70 (d, J=8.7 Hz, 1H, C[2]–H), 4.26 (t, J=7.6 Hz, 2H, C[7]–H), 4.19 (s, 4H, C[15–16]–H), 4.10 (q, J=7.1 Hz, 4H, C[19–20]–H), 4.02–3.95 (m, 8H, C[17–18, 21–22]–H), 3.04 (t, J=7.5 Hz, 2H, C[8]–H), 1.17 (t, J=7.1 Hz, 6H, C[23–24]–H), 1.07 (t, J=7.1 Hz, 6H, C[25–26]–H). ^{13}C {^{1}H} NMR (101 MHz, [D$_6$]DMSO) δ=190.8, 170.3, 170.2, 148.7, 144.5, 133.3, 130.6, 128.9, 127.1, 125.4, 124.6, 123.4, 116.0, 111.9, 68.3, 60.4, 60.2, 55.0, 53.8, 30.5, 29.1, 14.1, 14.0. HRMS (ESI+): *m/z* calcd for $C_{31}H_{41}N_2O_{10}^+$ ([M+H]$^+$): 601.27558, found: 601.27545.

The coupling to the fluorophore was carried out using the *General procedure 4* starting from 1 mmol starting material. The ethyl ester protected fluorescent dye **35** (yield: 50 mg, 6%) was isolated as a red powder. Melting point: decomposed at 118 °C. ^{1}H NMR (400 MHz, CDCl$_3$) δ=7.56 (d, J=9.3 Hz, 2H, C[33, 42]–H), 7.49–7.09 (m, 4H, C[2, 3, 11, 12]–H), 7.05–6.95 (m, 3H, C[5, 10, 13]–H), 6.94–6.83 (m, 4H, C[34, 36, 39, 41]–H), 4.35–4.29 (m, 8H, C[15–16, 19–

20]–H), 4.14 (t, J = 6.6 Hz, 2H, C[7]–H), 4.07–3.98 (m, 8H, C[17–18, 21–22]–H), 3.67 (q, J = 7.1 Hz, 8H, C[44–47]–H), 3.25 (t, J = 7.4 Hz, 2H, C[8]–H), 1.38 (td, J = 7.2, 1.8 Hz, 18H, C[23–24, 48–51]–H), 1.20 (t, J = 7.1 Hz, 6H, C[25–26]–H). ^{13}C {^{1}H} NMR (101 MHz, $CDCl_3$) δ = 190.8, 171.3, 170.7, 158.1, 155.4, 150.1, 149.0, 141.3, 133.7, 132.5, 130.8, 127.7, 125.3, 125.2, 124.5, 124.5, 123.2, 117.9, 114.6, 113.7, 113.3, 96.6, 61.2, 60.7, 55.1, 53.9, 46.1, 31.5, 14.4, 14.2, 12.7. HRMS (ESI+): *m/z* calcd for $C_{51}H_{65}N_4O_{10}^+$ ([M]$^+$): 893.46952, found: 893.46984.

The hydrolysis was carried out using *General procedure 5* starting from the quantities given above. The fluorescent dye **5b** (yield: 15 mg, 41%) was isolated as a red powder. Melting point: decomposed at 116 °C. ^{1}H NMR (400 MHz, [D$_4$]methanol) δ = 7.57 (d, J = 9.6 Hz, 2H, C[25, 34]–H), 7.28–7.23 (m, 2H, C[26, 33]–H), 7.13–6.96 (m, 7H, C[2–3, 5, 10–13]–H), 6.91 (d, J = 2.5 Hz, 2H, C[28, 31]–H), 4.38 (t, J = 7.5 Hz, 2H, C[7]–H), 4.23 (s, 4H, C[15–16]–H), 3.85 (s, 4H, C[17–18]–H), 3.66 (q, J = 7.1 Hz, 8H, C[36–39]–H), 3.19 (t, J = 7.6 Hz, 2H, C[8]–H), 1.29 (t, J = 7.1 Hz, 14H, C[40–43]–H). ^{13}C {^{1}H} NMR (101 MHz, [D$_4$]methanol) δ = 175.4, 174.2, 159.7, 159.5, 157.0, 151.2, 150.6, 142.8, 135.1, 133.8, 132.4, 128.5, 126.1, 125.7, 124.9, 124.4, 118.5, 116.9, 115.3, 114.5, 97.4, 70.4, 56.1, 55.4, 46.9, 33.1, 13.0. HRMS (ESI+): *m/z* calcd for $C_{43}H_{49}N_4O_{10}^+$ ([M]$^+$): 781.34432, found: 781.34423.

Preparation of the fluorescent dye 6b

The first step to achieve ethyl ester **20** was carried out following the previously reported method.[18] 1.72 g (43 mmol, 1.2 equiv.) NaH (60% in mineral oil) was suspended in 60 ml DMF, then 5 g (36 mmol, 1.0 equiv.) 2-nitrophenol in 10 ml DMF was added dropwise to this solution. The yellow solution of 2-nitrophenol turned into red/orange. The mixture was stirred at room temperature for 1 hour until the gas formation stopped, then 7.76 g (36 mmol, 1.0 equiv.) 2-nitrobenzyl bromide in 10 ml DMF was added dropwise. After stirring for 5 hours at 90 °C, the solution was cooled to room temperature and poured on crushed ice. The formed solids were filtered, and dried. The nitro compound **18** (yield: 9.0 g, 90%) was isolated as yellow crystals. Melting point: 153 °C. (Ref: 156 °C) The hydrogenation was carried out according to *general procedure 1*, with some modification. Only 5 bar H_2 was used, and 2 mol% PtO_2 proved to be an effective catalyst to terminate co-product formation. The amino compound **19** (brown crystal, yield: 3.0 g, 96%) was isolated starting from 4 g of **18**. Melting point: 96 °C. (Ref: 117 °C) The spectroscopic properties of compounds **18** and **19** were in agreement with those published previously.[17,28]

The alkylation was carried out according to *general procedure 2*, from 7 mmol of amine. The ethyl ester compound **20** (yield: 8.32 g, 87%) was isolated as a brown oil. ^{1}H NMR (400 MHz, [D$_6$]DMSO) δ = 7.37 (dd, *J* = 7.6, 1.6 Hz, 1H, C[12]–H), 7.30–7.16 (m, 2H, C[9, 11]–H), 7.06 (td, *J* = 7.3, 1.4 Hz, 1H, C[10]–H), 6.95 (dd, *J* = 7.5, 3.2 Hz, 1H, C[5]–H), 6.87–6.76 (m, 2H, C[3,4]–H), 6.70 (dd, *J* = 7.5, 3.2 Hz, 1H, C[2]–H), 5.06 (s, 2H, C[7]–H), 4.07 (s, 4H, C[14,15]–H), 4.04 (s, 4H, C[16,17]–H), 3.96 (q, *J* = 7.1 Hz, 4H, C[18,19]–H), 3.86 (q, *J* = 7.1 Hz, 4H, C[20,21]–H), 1.06–1.10 (t, *J* = 7.1 Hz, 12H, C[22–25]–H). ^{13}C {^{1}H} NMR (101 MHz, [D$_6$]DMSO) δ = 170.7, 170.5, 149.7, 149.4, 138.8, 131.0, 130.6, 128.5, 123.4, 122.0, 121.3, 120.8, 118.0, 113.2, 66.7, 60.1, 59.9, 54.8, 53.3, 14.0, 13.9. HRMS (ESI+): *m/z* calcd for $C_{29}H_{38}N_2O_9^+$ ([M+H]$^+$): 559.26501, found: 559.26552.

The formylation was performed according to *general procedure 3* using 3 mmol starting material. The aldehyde compound **29** (yield: 440 mg, 22%) was isolated as a yellow oil. ^{1}H NMR (400 MHz, [D$_6$]DMSO) δ = 9.74 (s, 1H, C[30]–H), 7.43–7.34 (m, 3H, C[3, 5, 9]–H), 7.27 (td, J = 7.7, 7.3, 1.7 Hz, 1H, C[11]–H), 7.21 (dd, J = 8.2, 1.3 Hz, 1H, C[12]–H), 7.07 (td, J = 7.3, 1.3 Hz, 1H, C[10]–H), 6.72 (d, J = 8.2 Hz, 1H, C[2]–H), 5.11 (s, 2H, C[7]–H), 4.14 (s, 4H, C[14–15]–H), 4.06 (s, 4H, C[16–17]–H), 3.95 (q, J = 7.1 Hz, 4H, C[18–19]–H), 3.82 (q, J = 7.1 Hz, 4H, C[20–21]–H), 1.07 (td, J = 6.6, 6.1, 2.9 Hz, 14H, C[22–25]–H). ^{13}C {^{1}H} NMR (101 MHz, [D$_6$]DMSO) δ = 190.7, 170.6, 170.2, 149.8, 148.7, 144.8, 131.3, 130.2, 128.9, 125.5, 123.5, 122.2, 116.0, 111.6, 67.1, 60.2, 60.2, 56.1, 54.8, 53.6, 14.0, 13.9. HRMS (ESI+): *m/z* calcd for $C_{30}H_{38}N_3O_9^+$ ([M+H]$^+$): 587.25993, found: 587.26038.

The coupling to the fluorophore was carried out using the *general procedure 4* starting from 0.38 mmol formyl compound. The ethyl ester protected fluorescent dye **36** (yield: 49 mg, 15%) was isolated as purple powder. Melting point: decomposed at 121.1 °C. ^{1}H NMR (400 MHz, $CDCl_3$) δ 7.45 (td, J = 8.2, 7.7, 3.1 Hz, 3H, C[3, 32, 41]–H), 7.30–7.24 (m, 2H, C[11, 12]–H), 7.18–7.13 (m, 1H, C[10]–H), 7.01 (d, J = 1.7 Hz, 1H, C[5]–H), 6.91–6.86 (m, 2H, C[35–38]–H), 6.85–6.77 (m, 4H, C[2, 9, 33, 40]–H), 5.20 (s, 2H, C[7]–H), 4.22 (s, 4H, C[14–15]–H), 4.05–3.96 (m, 8H, C[16–17, 18–19]–H), 3.93 (q, J = 7.1 Hz, 4H, C[20–21]–H), 3.63 (q, J = 7.1 Hz, 8H, C[43–46]–H), 1.34 (t, J = 7.0 Hz, 12H, C[47–50]–H), 1.23 (t, J = 7.1 Hz, 6H, C[22–23]–H), 1.14 (t, J = 7.1 Hz, 6H, C[24–25]–H). ^{13}C {^{1}H} NMR (101 MHz, $CDCl_3$) δ 171.3, 171.0, 158.2, 157.8, 155.3, 149.8, 149.5, 141.7, 132.6, 131.2, 131.0, 129.1, 124.7, 124.1, 123.7, 123.5, 117.4, 115.3, 113.7, 113.2, 96.6, 67.6, 61.1, 60.7, 55.1, 54.1, 46.1, 14.3, 14.2, 12.7. HRMS (ESI+): *m/z* calcd for $C_{50}H_{63}N_4O_{10}^+$ ([M]$^+$): 879.45387, found: 879.45421.

The hydrolysis was carried out using *general procedure 5* starting from the quantity given above. The fluorescent dye **6b** (yield: 40 mg, 94%) was isolated as a purple powder. Melting point: decomposed at 141 °C. ^{1}H NMR (400 MHz, [D$_6$]DMSO) δ = 12.88–11.98 (bs, 4H, C[18–21]OO–H), 7.40 (dd, J = 7.8, 1.7 Hz, 1H, C[5]–H), 7.32–7.26 (m, 1H, C[11]–H), 7.16–7.08 (m, 4H, C[9, 10, 24, 33]–H), 6.95–6.85 (m, 7H, C[2–3, 12, 25, 27, 30, 32]–H), 5.30 (s, 2H, C[7]–H), 4.23 (s, 4H, C[14–15]–H), 3.71 (s, 4H, C[16–17]–H), 3.62 (d, J = 7.4 Hz, 8H, C[35–38]–H), 1.20 (t, J = 7.0 Hz, 14H, C[39–42]–H). ^{13}C {^{1}H} NMR (101 MHz, [D$_6$]DMSO) δ = 172.2, 171.8, 157.4, 156.6, 154.6, 148.6, 147.8, 141.1, 131.8, 131.5, 128.2, 127.9, 123.9, 123.6, 123.0, 122.7, 117.0, 116.0, 114.0, 112.2, 96.0, 65.7, 54.4, 53.8, 45.2, 12.5. HRMS (ESI+): *m/z* calcd for $C_{42}H_{47}N_4O_{10}^+$ ([M]$^+$): 767.32867, found: 767.32667.

Preparation of the fluorescent dye 7b. (See Figure S2 in Supplementary Information)

The first step to achieve ethyl ester **23** was carried out following the previously reported method.[18] 2.4 g (60 mmol, 1.2 equiv.) NaH (60% in mineral oil) was suspended in 40 ml DMF, then 8.35 g (60 mmol, 1.2 equiv.) 2-nitrophenol in 30 ml DMF was added dropwise to this solution. The yellow solution of 2-nitrophenol turned into red/orange. The mixture was stirred at 60 °C for 30 minutes until the gas formation stopped, then 5.3 ml (7.15 g, 50 mmol, 1.0 equiv.) 2-fluoronitrobenzene was added. After stirring for 5 hours at 120 °C, the solution was cooled to room temperature and poured on crushed ice. The formed solids were filtered. The compound 2,2′-oxybis(nitrobenzene) (**S7**) (yield: 8.8 g, 68%) was isolated as a beige powder. The hydrogenation and alkylation steps were carried out according to the previously described *general procedures 1 and 2* (*vide supra*). The compound 2,2′-oxybis (aminobenzene) (**S8**) (brown solid, yield: 5.66 g, 92%) was isolated starting from 8 g of **S7**. The spectroscopic properties of compounds **S7** and **S8** were in agreement with those published earlier.[18] The ethyl ester compound **23** (brown crystals, yield: 11.70 g, 86%) was isolated starting from 5 g amine (**S8**). ^{1}H NMR (400 MHz, [D$_6$]DMSO) δ = 6.95 (td, *J* = 8.0, 1.6 Hz, 2H,C[3,10]–H), 6.81–6.71 (m, 4H, C-[2,4,9,11]–H), 6.63 (dd, *J* = 8.0, 1.6 Hz, 2H, C[5,8]–H), 4.17 (s, 8H, C[13–16]–H), 4.00 (q, *J* = 7.1 Hz, 8H, C[17–20]–H), 1.09 (t, *J* = 7.1 Hz, 12H, C[21–24]–H). ^{13}C {^{1}H} NMR (101 MHz, [D$_6$]DMSO) δ = 170.6, 148.0, 140.6, 123.7, 120.9, 120.5, 118.2, 60.1, 54.0, 14.0. HRMS

(ESI+): *m/z* calcd for $C_{28}H_{37}N_2O_9^+$ ([M+H]$^+$): 545.24936, found: 545.25068.

The formylation was performed according to *general procedure 3* starting from of 1.5 mmol of compound **23**. The aldehyde compound **30** (yield: 427 mg, 50%) was isolated as a green oil. ^{1}H NMR (400 MHz, [D$_6$]DMSO) δ = 9.62 (s, 1H, C[29]–H), 7.49 (dd, J = 8.5, 2.0 Hz, 1H, C[3]–H), 7.06–6.96 (m, 2H, C[5, 9]–H), 6.85–6.73 (m, 3H, C[2, 10, 11]–H), 6.62 (dd, J = 8.0, 1.6 Hz, 1H, C[8]–H), 4.32 (s, 4H, C[13–14]–H), 4.16 (s, 4H, C[15–16]–H), 3.99 (qd, J = 7.1, 4.0 Hz, 8H, C[17–20]–H), 1.11–1.05 (m, 12H, C[21–24]–H). ^{13}C {^{1}H} NMR (101 MHz, [D$_6$]DMSO) δ = 190.3, 170.6, 170.0, 147.1, 146.9, 145.8, 141.2, 128.3, 127.0, 124.6, 121.1, 120.9, 119.9, 118.2, 116.3, 60.4, 60.2, 56.1, 54.4, 54.0, 14.0, 13.9. HRMS (ESI+): *m/z* calcd for $C_{29}H_{37}N_2O_{10}^+$ ([M+H]$^+$): 573.24428, found: 573.24412.

The coupling to the fluorophore was carried out using the *general procedure 4* starting from 0.5 mmol of the formyl compound. The ethyl ester protected fluorescent dye **37** (yield: 104 mg, 24%) was isolated as a purple powder. Melting point: decomposed at 120 °C. 161.5–162.4 °C.^{1}H NMR (500 MHz, [D$_6$]DMSO) δ = 7.41 (d, J = 8.8 Hz, 2H, C[31, 40]–H), 7.12–7.04 (m, 3H, C[3, 32, 39]–H), 6.97 (td, J = 8.4, 5.9, 2.9 Hz, 1H, C[10]–H), 6.93 (d, J = 8.4 Hz, 1H, C[2]–H), 6.91–6.82 (m, 4H, C[8, 9, 34, 37]–H), 6.78 (d, J = 2.1 Hz, 1H, C[5]–H), 6.74 (d, J = 8.0 Hz, 1H, C[11]–H), 4.34 (s, 4H, C[13–14]–H), 4.17 (s, 4H, C[15–16]–H), 4.06 (q, J = 7.2 Hz, 4H, C[17–18]–H), 3.90 (q, J = 7.1 Hz, 4H, C[19–20]–H), 3.63 (q, J = 8.1, 7.6 Hz, 8H, C[42–45]–H), 1.19 (t, J = 7.0 Hz, 12H, C[46–49]–H), 1.12 (t, J = 7.0 Hz, 6H, C[21–22]–H), 1.04 (t, J = 7.1 Hz, 6H, C[23–24]–H). APT NMR (126 MHz, [D$_6$]DMSO) δ = 170.4, 157.8, 155.9, 154.8, 147.0, 146.6, 142.4, 138.9, 132.0, 125.2, 125.0, 122.5, 121.9, 121.3, 120.9, 118.6, 116.9, 115.6, 114.7, 114.0, 112.3, 95.9, 59.7, 54.3, 53.7, 45.9, 14.0, 13.9, 12.4. HRMS (ESI+): *m/z* calcd for $C_{49}H_{61}N_4O_{10}^+$ ([M]$^+$): 865.43822, found: 865.43896.

The hydrolysis was carried out using the *general procedure 5* using 0.05 mmol starting material. The fluorescent dye **7b** (yield: 35 mg, 93%) was isolated as a red powder. Melting point: decomposed at 161.5 °C. ^{1}H NMR (400 MHz, CD$_3$OD) δ = 7.61 (d, J = 9.5 Hz, 2H, C[23, 32]–H), 7.12–6. 90 (m, 6H, C[3, 8–10, 24, 31]–H), 6.87 (dd, J = 2.5, 9.5 Hz, 4H, C[2, 11, 26, 29]–H), 6.77 (d, J = 1.9 Hz, 1H, C[5]–H), 4.37 (s, 4H, C[13–14]–H), 4.19 (s, 4H, C[15–16]–H), 3.66 (q, J = 7.1 Hz, 8H, C[34–37]–H), 1.30 (t, J = 7.0 Hz, 12H, C[38–41]–H). ^{13}C {^{1}H} NMR (101 MHz, CD$_3$OD) δ = 175.1, 174.9, 159.5, 158.5, 156.8, 149.7, 148.4, 143.6, 143.6, 133.8, 126.5, 126.3, 124.9, 123.8, 123.0, 122.6, 119.7, 118.4, 115.0, 114.2, 97.2, 55.9, 55.3, 46.7, 12.8. HRMS (ESI+): *m/z* calcd for $C_{41}H_{45}N_4O_{10}^+$ ([M]$^+$): 753.31302, found: 753.31355.

Acknowledgements

This project was supported by the National Research, Development and Innovation Fund of Hungary, financed under the grant numbers 2018-1.1.2-KFI-2018-00097; 2018-1.3.1-VKE-2018-00032 and OTKA PD128612. The authors are grateful to the Hungarian Academy of Sciences for János Bolyai Research Fellowship [BO 21/799]. We thank Tamás Gáti (Department of Organic Chemistry, Semmelweis University, Budapest) for his assistance in spectroscopy measurements. We also thank Imre G. Csizmadia for providing critical remarks on the manuscript.

Conflict of Interest

The authors declare no conflict of interest.

Keywords: Calcium · Chelates · Density functional calculations · Dyes · Fluorescent probes

[1] M. J. Berridge, P. Lipp, M. D. Bootman, *Nat. Rev. Mol. Cell Biol.* **2000**, *1*, 11–21.
[2] R. Y. Tsien, *Biochemistry* **1980**, *19*, 2396–2404.
[3] C. Grienberger, A. Konnerth, *Neuron* **2012**, *73*, 862–885.
[4] J. T. Lock, I. Parker, I. F. Smith, *Cell Calcium* **2015**, *58*, 638–648.
[5] A. Barandov, B. B. Bartelle, C. G. Williamson, E. S. Loucks, S. J. Lippard, A. Jasanoff, *Nat. Commun.* **2019**, *10*, 1–9.
[6] K. Dhingra, P. Fousková, G. Angelovski, M. E. Maier, N. K. Logothetis, É. Tóth, *J. Biol. Inorg. Chem.* **2008**, *13*, 35–46.
[7] Z. Fu, Q. Fan, Y. Zhou, Y. Zhao, Z. He, *ACS Appl. Mater. Interfaces* **2019**, *11*, 39574–39585.
[8] M. J. Levene, D. A. Dombeck, K. A. Kasischke, R. P. Molloy, W. W. Webb, *J. Neurophysiol.* **2004**, *91*, 1908–1912.
[9] A. Takahashi, P. Camacho, J. D. Lechleiter, B. Herman, *Physiol. Rev.* **1999**, *79*, 1089–1125.
[10] R. Pethig, M. Kuhn, R. Payne, E. Adler, T. H. Chen, L. F. Jaffe, *Cell Calcium* **1989**, *10*, 491–498.
[11] T. Kimura, T. Maruyama, M. Okamura, T. Sugiyama, T. Ando, A. Ohno, *Bull. Chem. Soc. Jpn.* **1994**, *67*, 1615–1621.
[12] P. M. L. Robitaille, Z. Jiang, *Biochemistry* **1992**, *31*, 12585–12591.
[13] E. Andresen, S. Radunz, U. Resch-Genger, *New J. Chem.* **2021**, *45*, 13934–13940.
[14] "Database of Fluorescent Dyes, Properties and Applications," can be found under http://www.fluorophores.tugraz.at/substance/505, date accessed 01st september 2021.
[15] Z. Diwu, G. Haitao, P. Ruogu, Z. Qin, L. Jinfang, L. Feng, *Fluorogenic Calcium Ion Indicators and Methods of Using the Same*, **2017**, US-9810700-B1.
[16] I. C. S. Cardoso, A. L. Amorim, C. Queirós, S. C. Lopes, P. Gameiro, B. De Castro, M. Rangel, A. M. G. Silva, *Eur. J. Org. Chem.* **2012**, *2012*, 5810–5817.
[17] Y. Harry, S. Francis, *J. Med. Chem.* **1964**, *7*, 609–614.
[18] P. R. Ashton, B. Hörner, O. Kocian, S. Menzer, A. J. P. White, J. F. Stoddart, D. J. Williams, *Synthesis* **1996**, *1996*, 930–940.
[19] C. S. Lim, M. Y. Kang, J. H. Han, I. A. Danish, B. R. Cho, *Chem. Asian J.* **2011**, *6*, 2028–2033.
[20] J. R. Lakowicz, *Principles of Fluorescence Spectroscopy*, Springer, Boston, **2006**. p 51.
[21] R. Tsien, T. T. Pozzan, *Methods Enzymol.* **1989**, *172*, 230–262.
[22] In *Mol. Probes® Handb. – A Guid. to Fluoresc. Probes Labeling Technol. 11th Ed.*, **2010**.
[23] S. M. Harrison, D. M. Bers, *Biochim. Biophys. Acta – Gen. Subj.* **1987**, *925*, 133–143.
[24] M. J. Frisch, G. W. Trucks, H. B. Schlegel, G. E. Scuseria, M. A. Robb, J. R. Cheeseman, G. Scalmani, V. Barone, B. Mennucci, G. A. Petersson, H. Nakatsuji, M. Caricato, X. Li, H. P. Hratchian, A. F. Izmaylov, J. Bloino, G. Zheng, J. L. Sonnenberg, M. Hada, M. Ehara, K. Toyota, R. Fukuda, J. Hasegawa, M. Ishida, T. Nakajima, Y. Honda, O. Kitao, H. Nakai, T. Vreven, J. A. Montgomery Jr, J. E. Peralta, F. Ogliaro, M. Bearpark, J. J. Heyd, E. Brothers, K. N. Kudin, V. N. Staroverov, R. Kobayashi, J. Normand, K. Raghavachari, A. Rendell, J. C. Burant, S. S. Iyengar, J. Tomasi, M. Cossi, N. Rega, J. M. Millam, M. Klene, J. E. Knox, J. B. Cross, V. Bakken, C. Adamo, J. Jaramillo, R. Gomperts, R. E. Stratmann, O. Yazyev, A. J. Austin, R. Cammi, C. Pomelli, J. W. Ochterski, R. L. Martin, K. Morokuma, V. G. Zakrzewski, G. A. Voth, P. Salvador, J. J. Dannenberg, S. Dapprich, A. D. Daniels, Ö. Farkas, J. B. Foresman, J. V. Ortiz, J. Cioslowski, D. J. Fox, *Gaussian Inc Wallingford CT* **2016**.
[25] A. D. Becke, *J. Chem. Phys.* **1993**, *98*, 5648–5652.
[26] F. Vögtle, U. Heimann, *Chem. Ber.* **1978**, *111*, 2757–2764.
[27] R. A. Bounce, K. M. Easton, *Org. Prep. Proced. Int.* **2004**, *36*, 76–81.
[28] M. Hammerich, C. Schütt, C. Stähler, P. Lentes, F. Röhricht, R. Höppner, R. Herges, *J. Am. Chem. Soc.* **2016**, *138*, 13111–13114.

Manuscript received: August 5, 2021
Revised manuscript received: September 7, 2021
Accepted manuscript online: September 9, 2021